VŠB – Technical University of Ostrava

Faculty of Mechanical Engineering

Department of Applied Mechanics

DIPLOMA THESIS

DAMAGE ANALYSIS OF LOW CYCLE MULTIAXIAL FATIGUE UNDER PROPORTIONAL AND NON-PROPORTIONAL LOADING

Student: **VIKNESH ARTHANARIESWARAN HEMAMALINI**

Personal number: **ART0008**

Supervisor: **Dr. Ing. Ludmila Adámková**

Ostrava, 2021

VSB – Technical University of Ostrava
Faculty of Mechanical Engineering
Department of Applied Mechanics

Diploma Thesis Assignment

Student: **Viknesh Arthanarieswaran Hemamalini**

Study Programme: N2301 Mechanical Engineering

Study Branch: 3901T003 Applied Mechanics

Title: Damage Analysis of Low Cycle Multiaxial Fatigue under Proportional and Non-Proportional Loading
Analýza poškození nízkocyklovou únavou při proporcionálním a neproporcionálním zatěžování

The thesis language: English

Description:

1. Describe the problem of multiaxial low-cycle fatigue.
2. Explain the concepts of proportional and non-proportional loading.
3. Specify the most commonly used criteria of multiaxial fatigue.
4. Apply multiaxial fatigue criteria to specimen subjected to combined tension and torsion loading. Compare the results of different approaches.

References:

[1] Dowling,N.E. Mechanical behavior of materials. Engineering Methods for Deformation, Fracture and fatigue. Third edition. Pearson Prentice Hall,2007.
[2] Suresh, S. Fatigue of materials. Cambridge: Cambridge University Press, 1992, 621 p.
[3] De-Guang Shang, De-Jun Wang, Wei-Xing Yao. A Simple Approach to the Description of Multiaxial Cyclic Stress Strain Relationship.In.: International Journal of Fatigue 22 (2000),pp. 251–256.
[4] Jing Li, Zhong-Ping Zhang, Qiang Sun, Chun-Wang Li, Yan-Jiang Qiao. A New Multiaxial Fatigue Damage Model for Various Metallic Materials under the Combination of Tension and Torsion Loadings. In.: International Journal of Fatigue 31 (2009),pp.776–781.
[5] Ying-Yu Wang, Wei-Xing Yao: Evaluation and Comparison of Several Multiaxial Fatigue Criteria. In.: International Journal of Fatigue 26 (2004),pp. 17–25.

Extent and terms of a thesis are specified in directions for its elaboration that are opened to the public on the web sites of the faculty.

Supervisor: **Dr. Ing. Ludmila Adámková**

Date of issue: 18.12.2020

Date of submission: 17.05.2021

doc. Ing. Martin Fusek, Ph.D.
Head of Department

prof. Ing. Robert Čep, Ph.D.
Dean

Student's affidavit

I declare that I have prepared the whole diploma thesis, including appendices, independently under the leadership of the diploma thesis supervisor, and I stated all the documents and literature used.

In Ostrava on

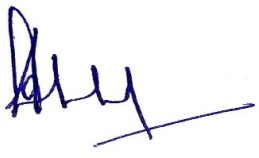

……..

Signature of Student

I declare that:

- I am aware that Act No. 121/2000 Coll, Act on copyright, rights related to copyright and amending some laws (the copyright Act), in particular, section 35(Use of a work in the civil or religious ceremonies or official events organized by public authorities, in the context of university performance and use of university work) and Section 60(university work) shall apply to my final Diploma thesis.
- I understand that VŠB- Technical University of Ostrava (hereinafter referred to as "VŠB-TUO") has the right to use this final Diploma thesis non-commercially for its internal use (Section 35 Subsection 3 of the Copyright Act)
- If requested, a copy of this Diploma thesis will be deposited with the thesis supervisor,
- if VŠB-TUO is interested, I will make a licensing agreement with it permitting to use the thesis within the scope of Section 12 Subsection 4 of the Copyright Act,
- I can only use my thesis, or grant a license to use it with the consent of VŠB-TUO, which is authorized in such a case to demand an appropriate contribution to the costs that were incurred by VŠB-TUO to create the thesis (up to the actual amount),
- I understand that - according to Act No. 111/1998 Coll., on higher education institutions and changes and amendments to other acts (Higher Education Act), as amended - that this Diploma thesis will be available for the public before the defense at the thesis supervisor's workplace, and electronically stored and published after the defense at the Central Library of VŠB-TUO, regardless of the outcome of its defense.

In Ostrava on

Viknesh Arthanarieswaran Hemamalini

Salem, Tamil Nadu, India

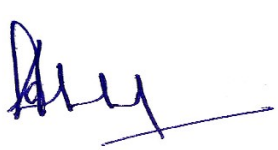

……..

Signature of Author

ANNOTATION OF MASTER THESIS

Viknesh Arthanarieswaran Hemamalini, Damage Analysis of Low Cycle Multiaxial Fatigue Under Proportional and Non-Proportional Loading. Ostrava: VSB - Technical University of Ostrava, Faculty of Mechanical Engineering, Department of Applied Mechanics, 2021,66p. Supervisor: Dr. Ing. Ludmila Adámková,

ABSTRACT

This thesis deals with the study of determination fatigue life of aluminum alloy AA2124-T851 prediction of materials at multiaxial fatigue. The first part of the thesis introduces uniaxial fatigue going to multiaxial fatigue. The next part focuses on the elaboration of separate criteria of multiaxial fatigue mainly for low-cycle fatigue for the estimation of life prediction of testing materials. Because the testing specimens were controlled strained at non-proportional low-cycle fatigue, these criteria were also selected in order to correspond with the given loading. The last part of this thesis is devoted to the evaluation of individual tests from different loading paths in the half of the life prediction of the component and following evaluation using specific criteria.

Keywords: Multiaxial Fatigue, Fatigue Life, Stress-Strain Relation, Proportional Loading, Non-Proportional Loading.

ANOTACE DIPLOMOVÉ PRÁCE

Viknesh Arthanarieswaran Hemamamlini. Analýza poškození nízkocyklovou únavou při proporcionálním a neproporcionálním zatěžování. Diplomová práce (in English). Ostrava: Vysoká škola báňská – Technická univerzita Ostrava, Fakulta strojní, Katedra aplikované mechaniky, 2021,66p. Vedoucí práce: Dr. Ing. Ludmila Adámková

ABSTRAKT

Diplomová práce se zabývá stanovením životnosti hliníkové slitiny AA2124-T851 v případě víceosé napjatosti. V první části diplomové práce je vysvětlena všeobecná problematika únavy materiálu a to jednak při jednoosé napjatosti a dále při napjatosti víceosé. Další část se zabývá stanovením únavové životnosti v případě porušení nízkocyklovou únavou. Cílem práce je stanovení životnosti zkušebních vzorků, zatěžovaných deformačně, a to jednak pro případy proporcionálního a neproporcionálního zatěžování. Jsou zde vysvětleny jednotlivé přístupy. V poslední části práce je provedeno vyhodnocení jednotlivých kritérií únavové životnosti a jejich srovnání s experimenty.

Klíčová slova: Multiaxiální únava, únavová životnost, napěťově-deformační vztahy, proporcionální zatěžování, neproporcionální zatěžování

CONTENTS

LIST OF FIGURES

LIST OF TABLES

LIST OF SYMBOLS

SYMBOL	DESCRIPTION	UNIT
b	Fatigue strength exponent	[-]
c	Fatigue ductility coefficient	[-]
Ќ	Strength coefficient	[MPa]
ń	Strain hardening exponent	[-]
A	Constant	[-]
B	Constant	[-]
E	Young modulus	[MPa]
G	Shear modulus	[MPa]
N_f	Number of cycles to fracture	[-]
$2N_T$	Transient number of cycles	[-]
σ_a	Stress amplitude	[MPa]
σ_u	Ultimate tensile stress	[MPa]
σ_e	Endurance limit	[MPa]
Y_e	Yield strength	[MPa]
S	Material constant	[-]
W	Density of deformation energy in the critical plane	[Jm^{-3}]
α	Angle of the critical plane	[rad]
γ_a	Shear strain amplitude	[-]
$\acute{\gamma}_f$	Shear fatigue ductility coefficient	[-]
γ_{xy}	Shear Strain in the xy plane	[-]
$\triangle\gamma$	Shear Strain range	[-]

$\triangle\gamma_{max}$	Maximum shear strain range	[-]
$\varepsilon_{ae}, \varepsilon_{ap}, \varepsilon_{ac}$	Total, elastic, plastic component amplitude of normal strain	[-]
$\acute{\varepsilon}_f$	Fatigue ductility coefficient	[-]
$\varepsilon_x, \varepsilon_y$	Normal strain in the X, Y direction	[-]
$\triangle\varepsilon_1$	Maximum principal of strain range	[-]
$\triangle\varepsilon_n$	Range of normal strain at the critical plane	[-]
ε_a	Normal strain amplitude	[-]
ν	Poisson's ratio	[-]
$\acute{\sigma}_f$	Fatigue strength coefficient	[MPa]
σ_m	Mean stress	[MPa]
σ_{nm}	Normal mean stress on the critical plane	[MPa]
$\sigma_{n,max}$	Maximum normal stress	[MPa]
$\sigma_{x,y}$	Normal stress in the X, Y direction	[MPa]
σ_{max}	Maximum stress	[MPa]
σ_{min}	Minimum stress	[MPa]
$\triangle\sigma_n$	Normal stress range	[MPa]
$\acute{\tau}_f$	Shear fatigue strength coefficient	[MPa]
$\triangle\tau$	Shear stress range	[MPa]
$\triangle\tau_1$	Shear stress range in the plane ε_{1max}	[MPa]
$\triangle\tau_{max}$	Range of maximum shear stress	[MPa]
φ	Phase angle	[rad]

1.INTRODUCTION

This diploma thesis deals with the criteria of multiaxial fatigue of the material supplemented by the experiment of specimens with different load trajectories. The experiment was performed for low-cycles fatigue or it was controlled by proportional and non-proportional loading of specimens. But first, we will be acquainted with the issue of materials fatigue during uniaxial stress, then we move on to the multiaxial stress that occurs in any machine or structure. Subsequently, the analysis of the criteria will be multiaxial fatigue for low cycle fatigue. These criteria contain mainly deformation members and for our experiment will be suitable. As there are countless of these criteria, individuals will be selected representatives of these criteria, which will be further subdivided according to the influencing parameter approach (deformation, energy). In this paper, an analysis of individual tests will be performed with the formation of the work was determination of fatigue life of some specimen for different loading cases and comparison with experiment by evaluating the data obtained from the experiment and assessing the results of the calculation of the selected one's criteria with measured values. Although most engineering structures and components are designed such that the nominal stress remains elastic, stress concentrations often cause plastic strains to develop within the vicinity of notches. Cyclic plastic strains lead to a material failure by low cycle fatigue (parts have a limited life). In the general case, the stress amplitude is variable and leads to variously great increments of plastic strain.

Multiaxial fatigue analysis, real loads can induce combined bending, torsional, axial, and shear stresses, which may be generated bi or tri-axial variable stress/strain histories at the juncture (in general a notch root), causing the so-called multiaxial fatigue problems.

This diploma thesis deals with the individual tests of shear strain-based multiaxial damage parameter to supported the predict the multiaxial fatigue life of using AA2124-T851 aluminum alloy.

2. FATIGUE OF MATERIALS

The machines and structure parts are often subjected to cyclic loading, which damages the microvolume of the material. With an increasing number of cycles, there's an accumulation of damage and therefore the fracture occurs when the stress is less than the yield strength of the materials Y_e. Damage and fracture due to the cyclic loading were described in 1839 by J.M. Poncelet fatigue of materials. Material fatigue is defined as the failure of a component subjected to cyclic loading. And also, fatigue is the most common cause of mechanical structure failure. It can be processed by until the materials finally fail under the repeated loading can be divided into three stages.[1][2]

- After a large number of cycles, the damage to develops on a microscopic level, and until it grows a macroscopic crack is formed.
- The macroscopic crack grows for every cycle until it reaches a critical length.
- The cracked component breaks since it cannot withstand the height load.

2.1 STRESS-BASED APPROACH

The stress-based approach load we encounter in the technical practice we can divide into two basic groups. It is, on the one hand, a deterministic loading, in which the magnitude of the stress can be determined according to exact relations, and on the other hand, a random loading. Deterministic loading can be periodic (usually harmonic) or non-periodic. In this chapter, we will deal only with the issue of cyclic periodic loading. In this case, we assume that the external forces and stresses usually change periodically from a certain minimum value (lower stress) to the maximum value (upper) stress. The course of the stress is usually represented by a sine function. The general course of the cyclic stress can be considered as a course caused by the superposition of the static component a_m and the stress amplitude σ_a. For such a case, the load cycle is defined. This is often illustrated by the figure:1 below.[2]

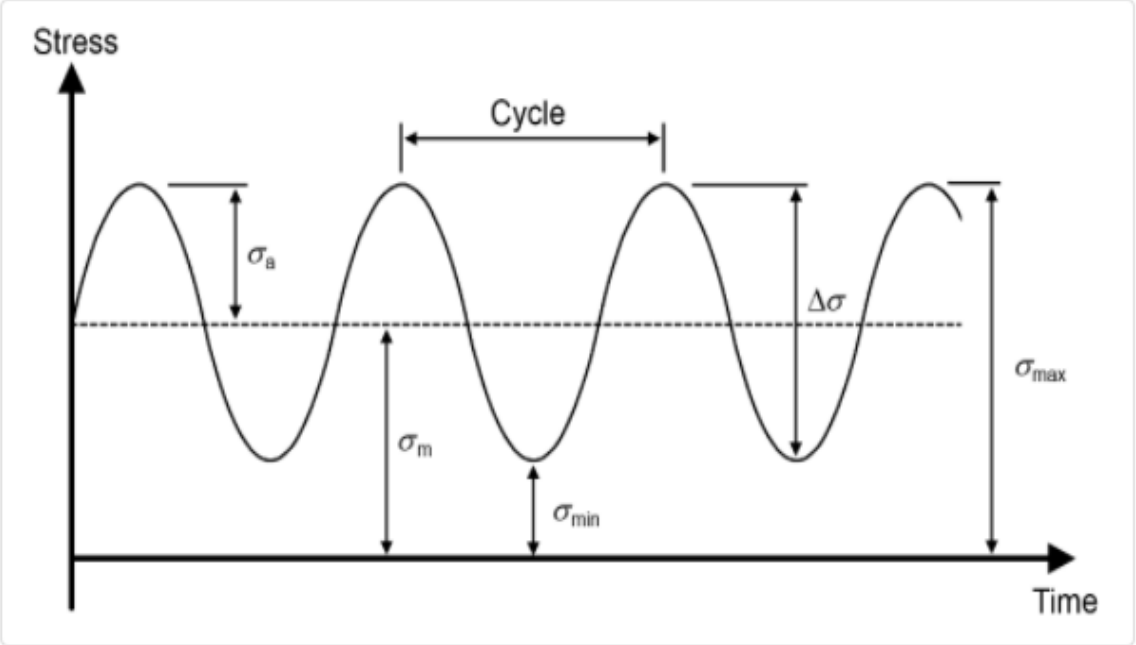

Figure 1 Cyclic Loading [1]

Mean stress σ_m and stress amplitude σ_a are given

$$\sigma_m = \frac{\sigma_{max}+\sigma_{min}}{2} \tag{2.1}$$

$$\sigma_a = \frac{\sigma_{max}-\sigma_{min}}{2} \tag{2.2}$$

And stress range $\Delta\sigma$ is given

$$\Delta\sigma = \sigma_{max} - \sigma_{min} = 2\,\sigma_a \tag{2.3}$$

Also, the following quantities are defined:

Stress ratio R

$$R = \frac{\sigma_{min}}{\sigma_{max}} = \frac{\sigma_m-\sigma_a}{\sigma_m+\sigma_a} \tag{2.4}$$

Hence

$$\sigma_a = \frac{\Delta\sigma}{2} = \frac{\sigma_{max}}{2}(1-R) \tag{2.5}$$

And

$$\sigma_m = \frac{\sigma_{max}}{2}(1+R) \tag{2.6}$$

2.2 FATIGUE LIMIT OF SMOOTH BODIES (WÖHLER CURVES)

By the effect of cyclic loading was first studied within the late 19th century by Augustus Wohler-studying problem of railway axle. About this characteristic, which was used by other research in the study of fatigue properties of the material, August Wohler he deserved his experimental investigation of the rail axle failures during cyclic loading. It had been necessary to explain why under cyclic loading materials breaches at stress less than the yield limit without causing the plastic deformations. During the test specimens are loaded with the stress amplitude and determines the number of cycles to failure. By using materials fatigue data are often given for the two types of load: fully reversed and repeated. Again, by using the test specimen shall be of an equivalent material, have an equivalent shape, and be well worked. Usually, it's a test rods diameter the 7 ÷ 10mm with a polished surface.[4]

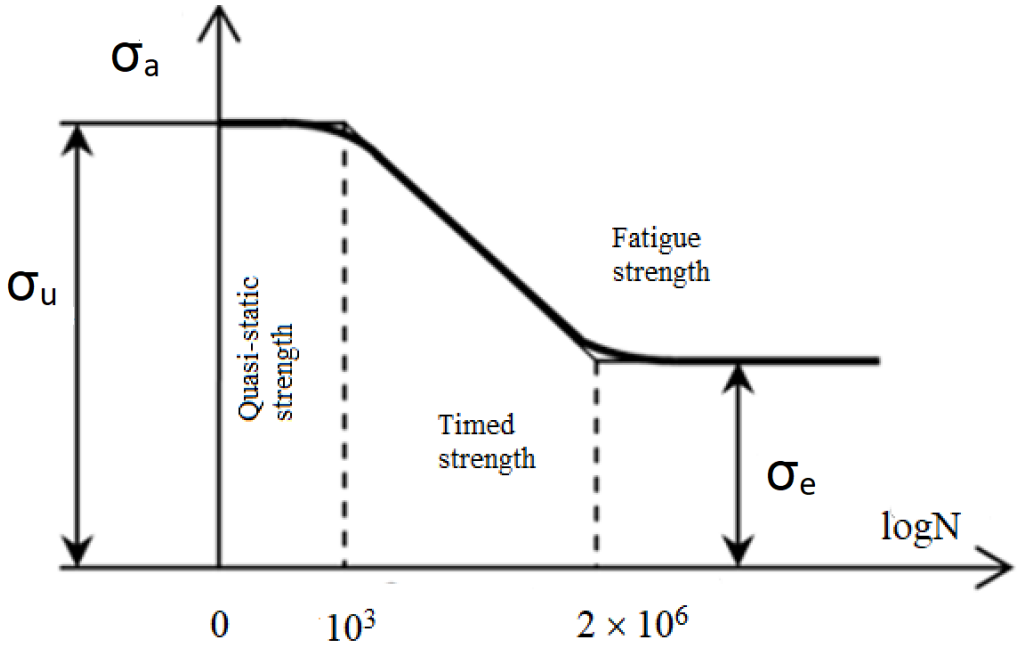

Figure 2 Wohler Curve [4]

The Wohler curve indicates the dependence of the stress amplitude on the number of cycles N_f to failure. The curve shows that as the number of cycles rises, the value of the stress amplitude falls to the fatigue limit of the material. According to the number of cycles, the curve is divided into an area of low cycles fatigue (hereinafter referred to as LCF), which is the most often observed in the range of $N_f = 10^3$-10^4 cycles and there is plastic deformation throughout the whole-body volume during microcracks and the area of high-cycles fatigue (hereinafter referred to as HCF), which reaches a higher lifetime than 10^5 cycles and plastic deformation is

accumulated at the site of crack initiation. The most general method to present the test result is to plot a graph with the stress amplitude on the coordinate(y-axis) versus the logarithm of the number of cycles N to fatigue failure on the absicsa (x-axis). In the Wohler curve can be divided into three categories.

- Region 1: When the number of cycles is small, is it an area of quasi-static fractures (N ≅ 10^3 cycles).
- Region 2: The time area in which the stress amplitude decreases. This is the so-called time strength with a limited lifetime.
- Region 3: Approximately N ≥ 2× 10^6 cycles, the last area where the stress amplitude is constant, we are talking about the so-called unlimited service lifetime.

For the area LCF and HCF, the service lifetime of the test specimens for uniaxial stress can be expressed using the Basquin relation.

The life curve can be described as the dependence of the number of cycles to failure N_f on the stress amplitude σ_a:

$$\sigma_a = \sigma_f'(2N_f)^b \tag{2.7}$$

Where σ_f' is the fatigue strength coefficient and b is the fatigue strength exponent.

2.3 STRAIN BASED APPROACH

The strain-based approach to fatigue considers the plastic deformation which will occur in localized regions where fatigue cracks begin, such as at beam edges and stress raisers, stresses and strains in such region are analyzed and used because the basis for all times estimates. This procedure permits detailed consideration of fatigue situations where local yielding is involved, which is usually the case for ductile metals at relatively short lives. The method, however the approach also applies where there is little plasticity at long lives, so that it's a comprehensive approach that will replace the stress-based approach.[2]

And another important curve characterizing the uniaxial stress in during cyclic loading in the LCF is the Manson-Coffin curve. The Manson-Coffin independently expressed by the relationship between the amplitude of plastic deformation and the number of cycles to failure.

$$\varepsilon_{ap} = \varepsilon_f'(2N_f)^c \tag{2.8}$$

Where ε_f' is the fatigue ductility coefficient, which is the given by extrapolation of ε_{ap} in the first load cycle ($2N_f = 1$) and c is the fatigue ductility exponent.

Depending on the amplitude of the total deformation of the ε_{ac} and the lifetime of the component, it is possible to express relation among total strain amplitude ε_{ac} and fatigue life N_f number of cycles.

$$\varepsilon_{ac} = \varepsilon_{ae} + \varepsilon_{ap} = \frac{\sigma_f'}{E}(2N_f)^b + \varepsilon_f'(2N_f)^c \tag{2.9}$$

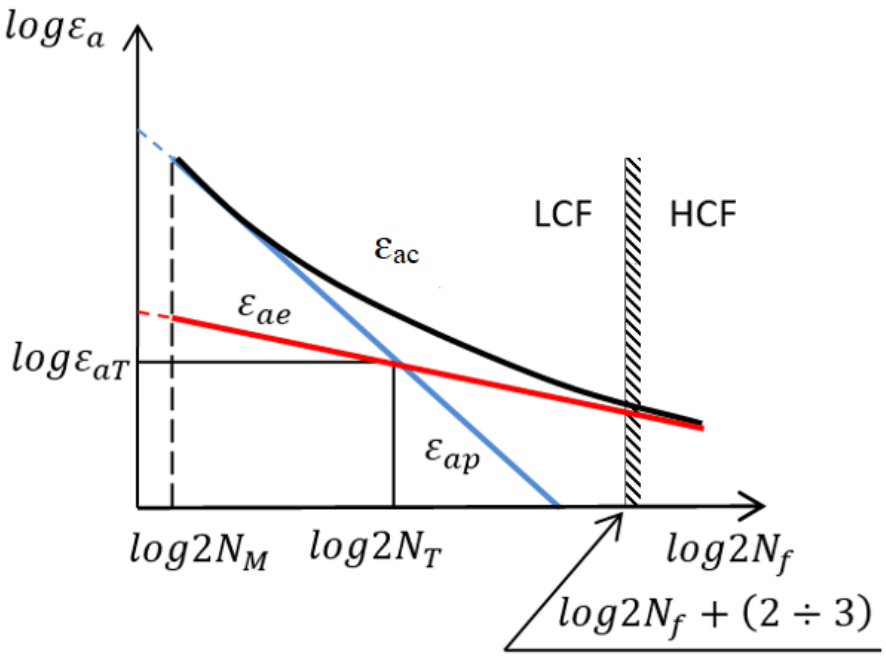

Figure 3 Relation between strain amplitude and fatigue life [4]

For elastic strain amplitude ε_{ae} Basquin relation is valid.

In the logarithmic coordinates are the Manson-Coffin and Basquin curves are displayed as a straight line. At their intersection, there is a transient number of cycles of 2NT is reached, which separated the fatigue region with predominant plastic deformation from the region with predominant elastic deformation.

3. FATIGUE DAMAGE PHASE

Fatigue fracture is the result of crack initialization, which leads to further crack propagation to materials limit state. These phases can be divided into four groups.

- Change in the mechanical properties of the materials.
- Crack initiation
- Crack propagation.
- Ultimate failure.

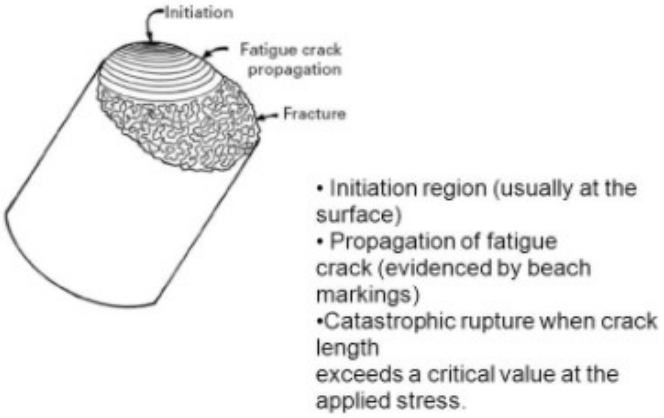

Figure 4 Stages of Fatigue Damage [3]

The different stages of life do not have set boundaries, so there may be an interweave in the individual phase.

3.1 CHANGE IN THE MECHANICAL PROPERTIES OF THE MATERIALS

During cyclic loading, where the stress and strain deformation exceeds the yield strength of the materials limit, there are changes in the properties of the material, both mechanical and physical. The change in the mechanical properties of the material is manifested by changes in the hysteresis loops. The peaks of individual hysteresis loops at different values of stress amplitude can be intersected by a curve called a cyclic deformation curve see. Figure:5

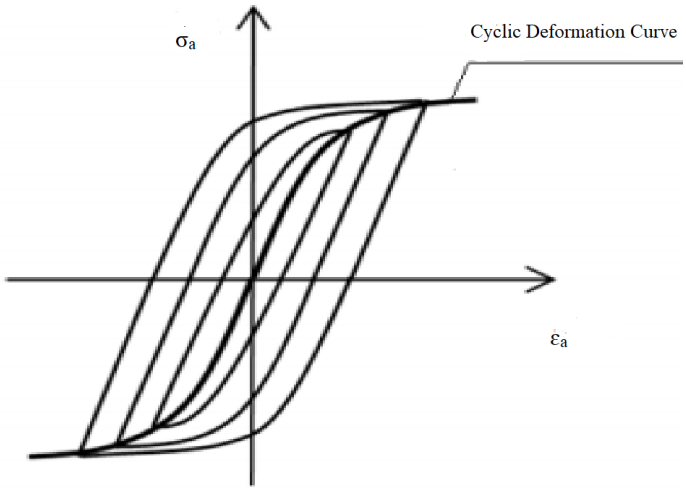

Figure 5 Steady-State Cyclic Deformation Curve [4]

Throughout the whole range, we approximate this curve using the relation.

$$\sigma_a = \acute{K}\varepsilon_{ap}^{\dot{n}} \tag{3.1}$$

Where K' is the strength coefficient and n' is the strain hardening exponent. Further σ_f' it expresses the fatigue strength coefficient and ε_f' is the fatigue ductility coefficient. This relationship also determines the dependence of the stress amplitude on the plastic deformation. This can be used for a stable hysteresis loops see Figure:6. Where the height of the hysteresis loop is become twice the values of the amplitude of stress and the width of twice the amplitude of plastic deformation.

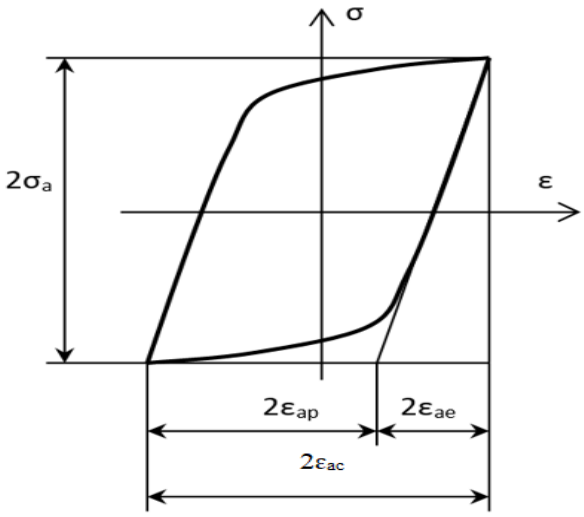

Figure 6 Steady Hysteresis Loop [4]

This hysteresis loop only applies to uniaxial stress. For our case multiaxial stress, it is necessary to choose the suitable multiaxial criteria to determine the prediction of life, which will be discussed about chapter 5.

According to the method of stress the tested specimens and their response to cyclic stress, we divided them into two idealized states.

- Constant Strain Range △ε=const.
- Constant Stress Range △σ=const.

3.1.1 CONSTANT STRAIN RANGE △ε = Const

Constant strain range, is also referred to as hard loading. This idealized state was used in our testing of specimens at the LCF.

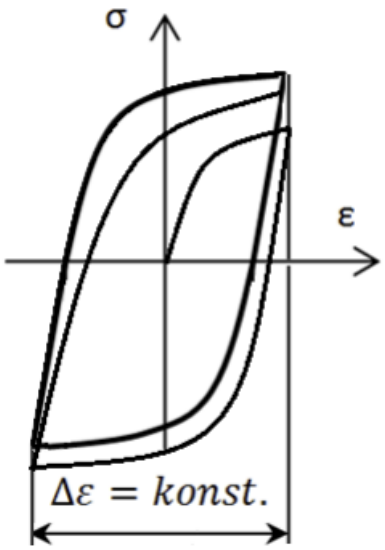

Figure 7 Hard Loading [4]

In the case of LCF under hard loading, the behavior of the material is characterized by a closed hysteresis loop, which during the first load cycle is a characteristic of the stress-strain dependence taken according to a static curve see Figure:8. Then shows the calculation of the total deformation $\varepsilon_{ac.}$

$$\varepsilon_{ac} = \varepsilon_{ae} + \varepsilon_{ap} = \frac{\sigma_a}{E} + \left(\frac{\sigma_a}{K'}\right)^{\frac{1}{n'}} \tag{3.2}$$

During further loading of the material, the mechanical properties are change, namely either hardening or softening. Therefore, this cyclic curve will be above the static curve.

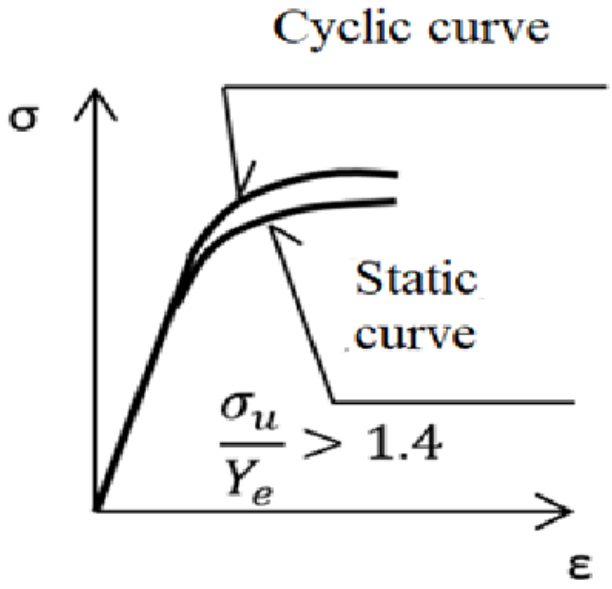

Figure 8 Cyclic Hardening [4]

Otherwise, the stress amplitude decreases, and therefore this cyclic curve is below static curve.

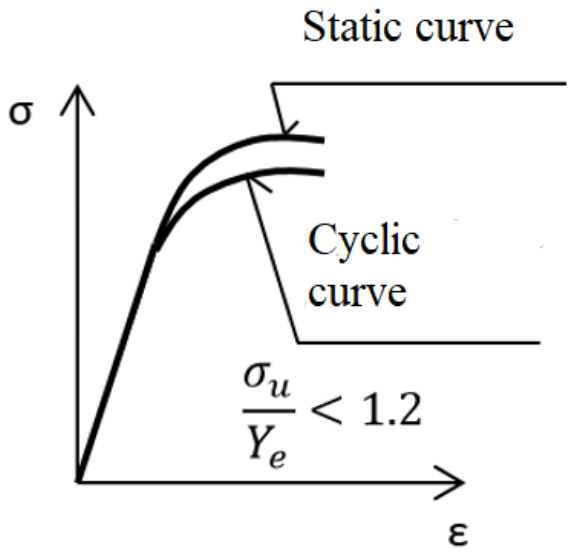

Figure 9 Cyclic Softening [4]

Experiments have shown that materials that are pre-reinforced undergo cyclic softening during the fatigue process. On the conversely, soft materials are cyclically reinforced during the fatigue process.

3.1.2 CONSTANT STRESS RANGE $\triangle\sigma$ = Const

Constant stress range is referred to as soft loading. For our case, this condition was unusable, so we will not discuss it further.

The most important factor in both idealized states is the component of mean stress σ_m. If this component is equal to zero, both cases described leading to the same lifetime for using the same empirical formula. However, if the mean stress is non-zero, there ratchening will occur. This leads to a significant impact on service life and is inadmissible for dimensioned structures.

3.2 CRACK INITIATION

Crack initiation, where in a small crack forms at some point of high-stress concentration. Fatigue crack initiation occurs mainly on the surface of the test specimen than inside. Cracks associated with fatigue failure almost always initiate on the surface of a component at some point of stress concentration. Let us distinguish three types of initiation of crack. The first type is fatigue slip zones. The second type is the boundaries of crystalline grain, which limit the continuity of deformations and apply at higher temperatures. The third type of initiation site is the boundary between the matrix and the non-metallic inclusion. The most common nucleation zones are slip zones, the formation of which usually also precedes nucleation near the grain boundaries and in the range of non-metallic inclusion and the matrices. If there is a slip in one slip plane of the crystalline steel grain, it will be strengthened so that another slip occurs in the adjacent plane. On the surface of a cyclically loaded specimen, so-called intrusion and extrusion occur Figure:10, which end on the fatigue slip zones on the surface of the part. The resulting micro-screws act as stress concentrators and microcracks are formed and spread here.[5][6]

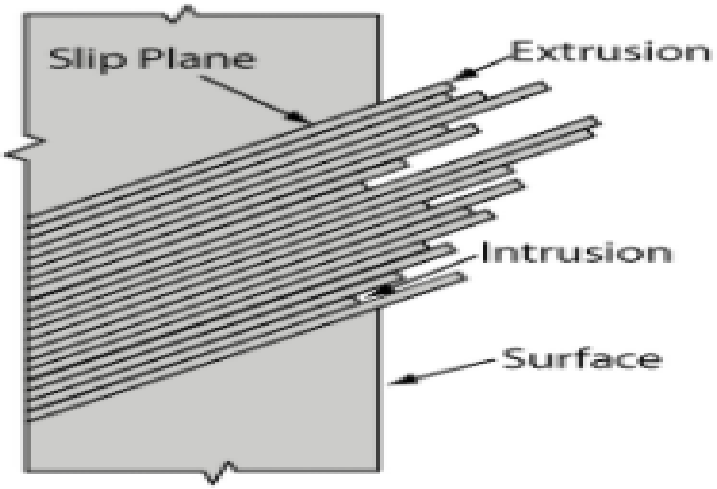

Figure 10 Formation of Intrusion and Extrusion [6]

3.3 CRACK PROPAGATION

Crack propagation is a process in which this crack grows in size with each stress cycle. In the site of the largest accumulation of microcracks, they are combining into longer cracks, following the slip planes of the individual grains in a direction perpendicular to the direction of the principal stress. After reaching a sufficient length, the microcracks begin to spread to the depth of the specimen below the surface. The resulting microcracks continue to grow until due to the uneven distribution of stress and strain, some of the cracks become a controlling crack. This crack will then grow on a large part of the specimen, while the remaining cracks suppressed their growth.[5]

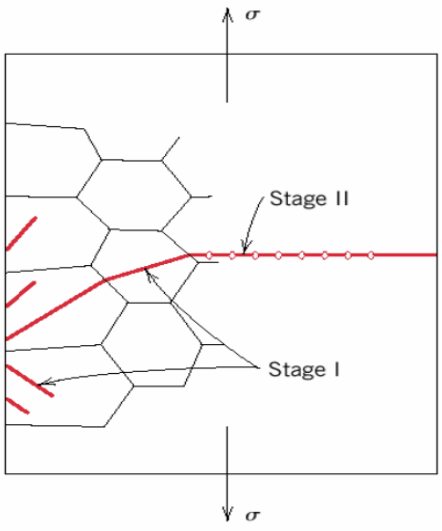

Figure 11 Crack Propagation [7]

3.4 FINAL FAILURE

The last phase of fatigue damage is the final sudden fracture. The nature of this fracture varies according the operating temperature and also the resistance of the materials to brittle fracture.

Figure 12 Final Failure [8]

4. MULTIAXIAL FATIGUE

In real parts of machines and steel structures, there is a stress of multiaxial, which can lead to the emergency situations. Problem of multiaxial loading are at technical practice for example – combined loading tension and torsion, bending and torsion, pressure vessel and similarly.

From this situation stress tensor definition is valid

For 2- dimensional (plane problem)

$$T_\sigma = \begin{bmatrix} \sigma_x & \tau_{yx} \\ \tau_{xy} & \sigma_y \end{bmatrix} \tag{4.1}$$

Where σ_x, σ_y, and τ_{yx} are the time dependence variables.

For combined loading the tension and torsion, where $\sigma_x = \sigma_t$, $\sigma_y = 0$ and $\tau_{xy} = \tau_t$.

We receive

$$T_\sigma = \begin{bmatrix} \sigma_x & \tau_{yx} \\ \tau_{xy} & 0 \end{bmatrix} \tag{4.2}$$

Similarly strain tensor is defined

$$T_\varepsilon = \begin{bmatrix} \varepsilon_x & \frac{\gamma_{XY}}{2} & \frac{\gamma_{XZ}}{2} \\ \frac{\gamma_{XY}}{2} & \varepsilon_Y & \frac{\gamma_{YZ}}{2} \\ \frac{\gamma_{XZ}}{2} & \frac{\gamma_{YZ}}{2} & \varepsilon_Z \end{bmatrix} \tag{4.3}$$

For tension and torsion combined loading we will receive

$\gamma_{xz} = \gamma_{yz} = 0$

$\varepsilon_y = \varepsilon_z = -\nu_{ef}.\varepsilon_x$

$$T_\varepsilon = \begin{bmatrix} \varepsilon_x & 1/2\gamma_{xy} & 0 \\ 1/2\gamma_{xy} & -\nu_{ef}\varepsilon_x & 0 \\ 0 & 0 & -\nu_{ef}\varepsilon_x \end{bmatrix} \tag{4.4}$$

Where ν_{ef} effective Poisson's ratio

A specimen used for the multiaxial fatigue test for tension-torsion is shown schematically in Figure:13. The applied strain could also be given by the following strain tensor under strain-controlled loading conditions.[10]

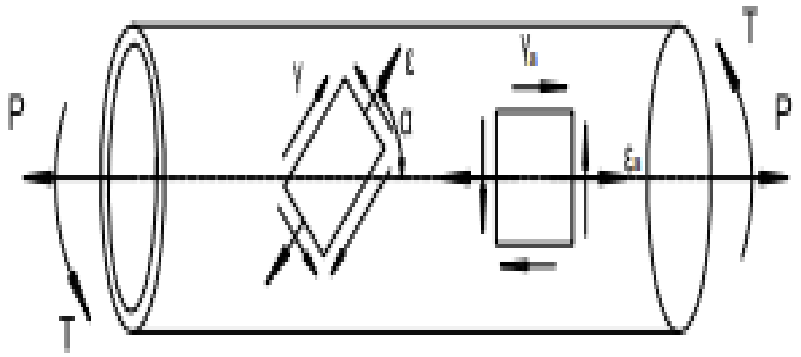

Figure 13 Strain state of the Tension-Torsion Specimen [9]

If the applied loading is sin wave, i.e.

$$\varepsilon_x = \varepsilon_a \sin \omega t \tag{4.5}$$

$$\gamma_{xy} = \gamma_a \sin(\omega t - \varphi) \tag{4.6}$$

Where

ε_a – Normal strain amplitude,

γ_a – Shear strain amplitude,

φ – Phase angle,

4.1 STRESS COMPONENT ON INCLINED PLANE

The normal and shear strains on the plane that form an angle α with the specimen axis are expressed as.

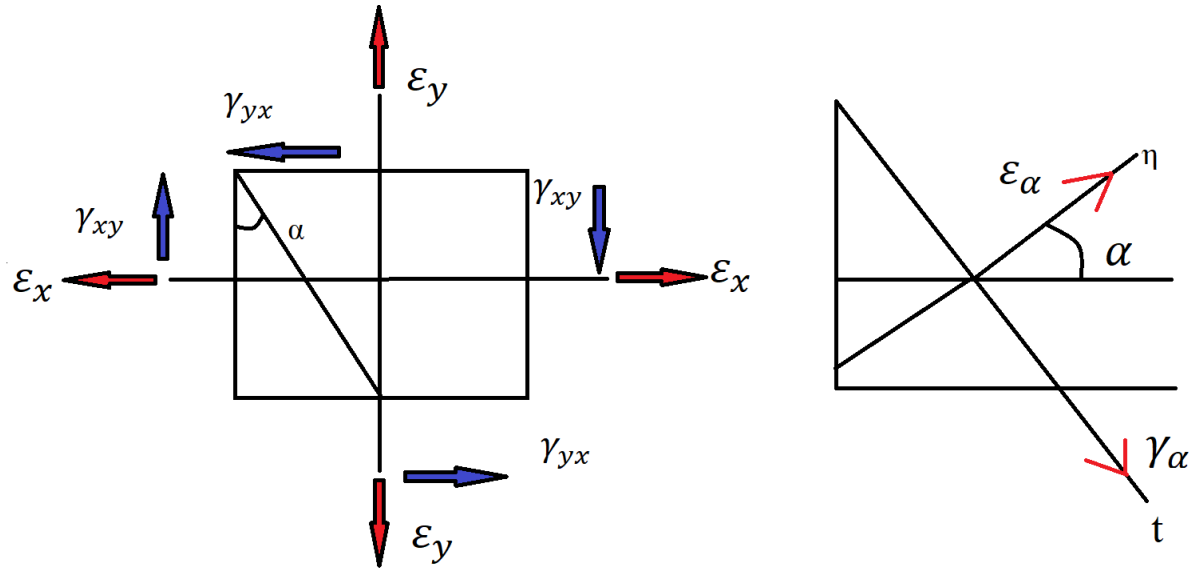

Figure 14 Strain Transformation and Inclined Plane with Similarly

From this figure we can determine[10]

$$\varepsilon_\alpha = \frac{1-\nu}{2}\varepsilon_x + \frac{1+\nu}{2}\varepsilon_x \cos 2\alpha + \frac{1}{2}\gamma_{xy}\sin 2\alpha \quad (4.7)$$

$$\gamma_\alpha = -(1+\nu)\varepsilon_x \sin 2\alpha + \gamma_{xy}\cos 2\alpha \quad (4.8)$$

Where ε_x and γ_{xy} are the axial and shear strain, respectively, ν_{eff} is the effective Poisson's ratio. Which is given by

$$\nu_{eff} = 0.5 - \frac{(0.5-\nu_e)\Delta\sigma_{eq}}{E\Delta\varepsilon_{eq}} \quad (4.9)$$

where ν_e is the elastic Poisson's ratio, E is the elastic modulus, $\triangle\sigma_{eq}$ and $\triangle\varepsilon_{eq}$ are the Von-Mises equivalent stress and strain ranges, respectively.

Equation can be derived from it (4.5) – (4.8) that

$$\varepsilon_\alpha = \frac{1}{2}\varepsilon_a \{[2(1+\nu)\cos^2\alpha - 2\nu + \lambda \sin 2\alpha \cos\varphi]^2 + [\lambda \sin 2\alpha \sin\varphi]^2\}^{1/2}\sin(\omega t - \xi) \quad (4.10)$$

$$\gamma_\alpha = \varepsilon_a \{[\lambda \cos 2\alpha \cos\varphi - (1+\nu)\sin 2\alpha]^2 + [\lambda \cos 2\alpha \sin\varphi]^2\}^{1/2}\sin(\omega t - \eta) \quad (4.11)$$

Where

$$\xi = \arctan\{ \lambda \sin 2\alpha \sin \varphi/[(1+\nu) \cos 2\alpha]+[(1-\nu) +\lambda \sin 2\alpha \cos \varphi]\} \quad (4.12)$$

$$\eta = \arctan\{-\lambda \cos 2\alpha \varphi/[\lambda \cos 2\alpha \cos \varphi - (1+\nu)\sin 2\alpha]\} \quad (4.13)$$

$$\lambda = \gamma_a/\varepsilon_a \quad (4.14)$$

γ is differentiated in relation to α which gives the maximum or minimum value of angle α for the shear strain.

$$\frac{\partial \gamma_\alpha}{\partial \alpha} = 0 \quad (4.15)$$

After we will receive

$$\alpha_m = \frac{1}{4} \arctan [2\lambda(1+\nu) \cos \varphi]/[1+\nu)^2-\lambda^2] \quad (4.16)$$

By replacing equation (4.16) into equation (4.10) and (4.11) the differential function for the maximum value γ_{max} by the shear strain and normal strain ε_n on the maximum shear plane is configured by.

$$\gamma_{max}(t) = \gamma_{max} \sin(\omega t + \eta) \quad (4.17)$$

$$\varepsilon_n(t) = \varepsilon_n \sin(\omega t + \xi) \quad (4.18)$$

Where the range of $\xi+ \eta$ is between $\frac{-\pi}{2}$ and $\frac{\pi}{2}$.

From the technical practice two basic problem exist

- Proportional Loading
- Non-proportional Loading

4.1.1 PROPORTIONAL LOADING

The direction of the principal stresses is constant during the loading cycle. From this reason phase angle among normal strain ε and shear strain γ components are zero.

Phase angle φ=0

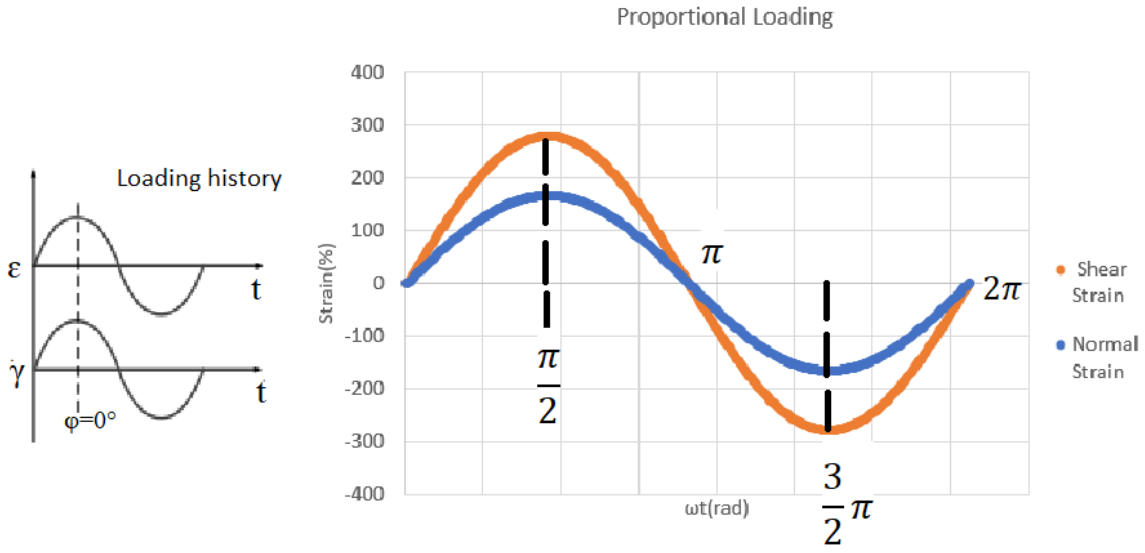

Figure 15 Proportional Loading- for Specimen C3

4.1.2 NON-PROPORTIONAL LOADING

The principal axes rotate during cyclic loading, non-zero phase angle exists among normal strain ε and shear strain γ components. This figure:16 shows non-proportional loading cases H -Phase angle φ=45°.

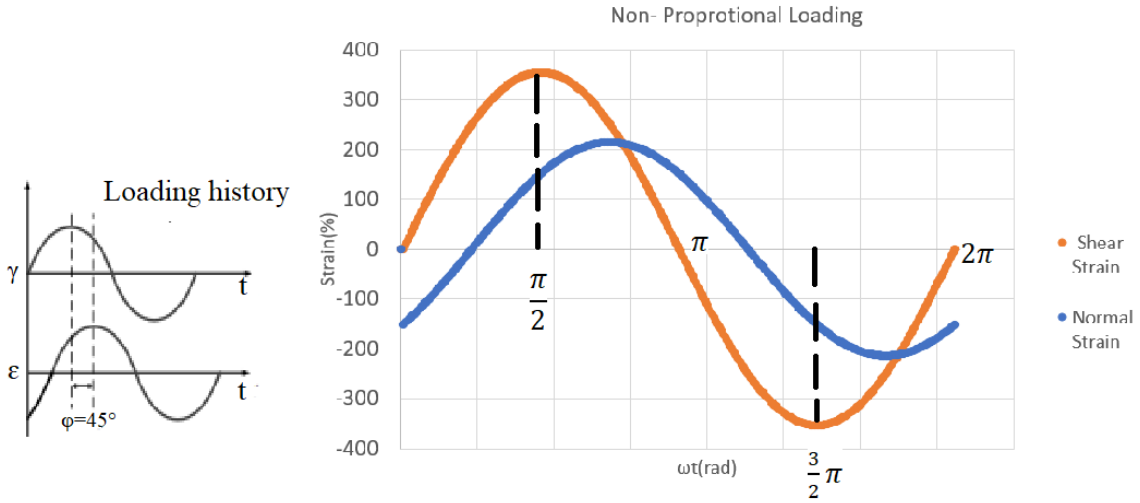

Figure 16 Non-Proportional Loading-for Specimen H3

5. EXPERIMENT

Part of the diploma thesis was the examination of a specimen of aluminum alloy AA2124-T851. Specimens were cyclically loaded by combination push-pull and torsion at the LCF with phase shifts φ between the component tensile and shear, so it was a non-proportional load. One test took place at proportional stress by a combination of push-pull and torsion, so the phase shift was zero. Depending on the magnitude of the phase shift, 5 different load trajectories were created. Eight specimens were tested in each trajectory. Some of the above were applied to selected specimens' multiaxial criteria with the calculation of the life of the specimens and a comparison with the experiment.

The chemical composition of this aluminum alloy and monotonic mechanical properties are shown in Table 1, and 2 respectively.

Table 1 Chemical Composition of the Aluminum Alloy AA2124-T851(%)

Si	**Fe**	**Cu**	**Mn**	**Mg**	**Cr**	**Zn**	**Ti**
0.2	0.3	4.9	0.9	1.8	0.1	0.25	0.15

Tensile strength	σ_u (MPa)	473
Yield strength	Ye (MPa)	435
Young modulus	E (GPa)	206
Poisson's ratio	ν (-)	0.3
Shear modulus	G (MPa)	44965

Table 2 Monotonic Mechanical Properties of the Material Studied

5.1 DESCRIPTION OF THE TEST SPECIMEN

Testing of Low-cycle fatigue specimen under proportional and non-proportional loading took place on a testing machine. The hollow cylindrical pattern with an outer diameter of 12.5mm and an inner diameter of 10mm was used. The cycle properties obtained by fitting the test results are shown in Table 3. The geometry and dimension of the specimen are shown in Figure: 17.

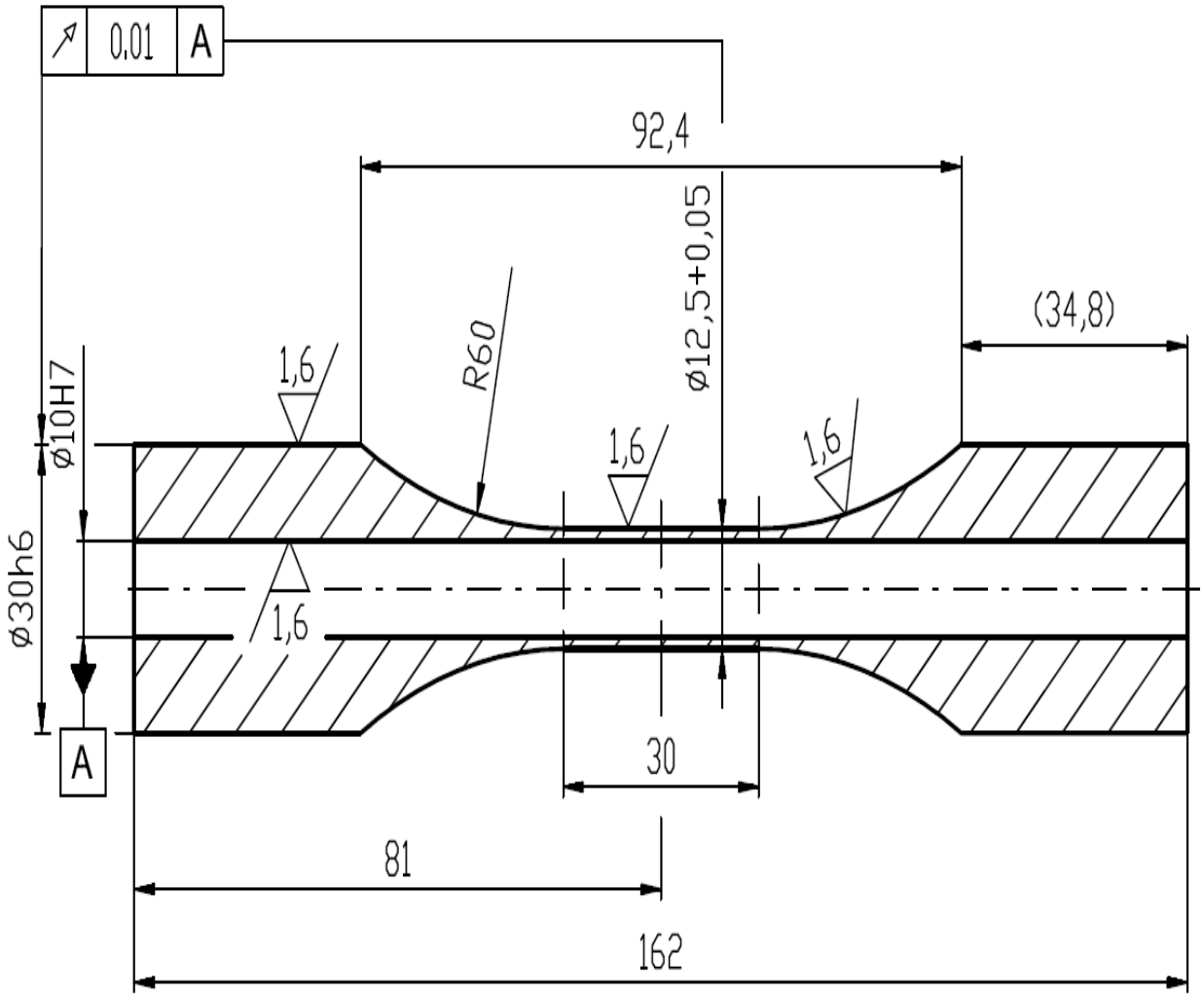

Figure 17 Specimen Geometry for Biaxial Cyclic Push-Pull and Torsion

Cyclic Properties	Push-Pull		Torsion	
Young modulus	E[MPa]	65540	G[MPa]	26700
Strength coefficient	K'[MPa]	646	$K_\gamma{}'$[MPa]	406
Fatigue strength coefficient	σ_f' [MPa]	611	τ_f' [MPa]	400
Fatigue ductility coefficient	ε_f' [−]	0.529	γ_f' [−]	0.875
Fatigue strength exponent	b [−]	-0.063	b_γ [−]	-0.0978
Fatigue ductility exponent	c[−]	-0.706	c_γ [−]	-0.874
Strain hardening exponent	n'[−]	0.0892	n_γ'[−]	0.111

Table 3 Cyclic Properties of AA2124-T851

5.2 TEST RESULT

Specimen number	ε_a	σ_a [MPa]	γ_a	τ_a [MPa]	N_f
A1	0.02	444	0	0	67
A2	0.015	424	0	0	209
A3	0.01	389	0	0	642
A4	0.008	370	0	0	1206
A5	0.0065	358	0	0	3194
A6	0.0055	328	0	0	7062
B1	0	0	0.0264	253	41
B2	0	0	0.0218	240	85
B3	0	0	0.0135	230	152
B4	0	0	0.0104	215	322
B5	0	0	0.00730	183	2257
B6	0	0	0.00630	164	6800
C1	0.00889	323	0.0154	179	165
C2	0.00731	301	0.0127	174	226
C3	0.00549	279	0.00951	166	704
C4	0.00353	238	0.0055	151	2270
C5	0.00282	210	0.00488	134	1268
C6	0.00245	184	0.00425	121	2765
G1	0.00998	427	0.0173	241	74
G2	0.00747	394	0.0129	229	135
G3	0.00648	373	0.0112	214	240
G4	0.00551	351	0.00954	204	352
G5	0.00451	318	0.00782	188	1580
G6	0.00308	234	0.00533	144	1445
H1	0.00998	396	0.0173	242	70
H2	0.00748	370	0.0130	224	146
H3	0.00646	354	0.0112	214	396
H4	0.00498	323	0.00862	191	874
H5	0.00423	293	0.00732	178	1912
H6	0.006335	260	0.00607	160	5360

Figure 18 Fatigue Test Data for Aluminum Alloy2124-T851

5.2.1 SPECIFY LOADING PATHS

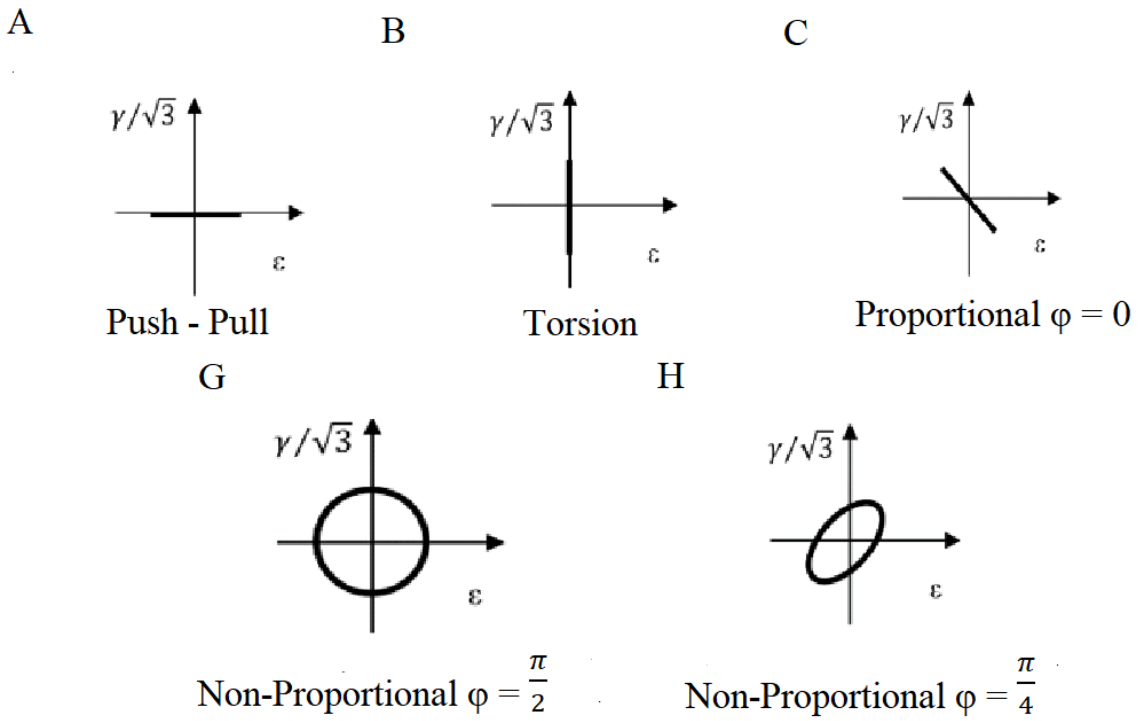

Figure 19 Multiaxial Fatigue Loading Paths [11]

5.3 DETERMINATION OF FATIGUE LIFE-UNDER MULTIAXIAL STRESS- STRAIN BEHAVIOUR

Fatigue under multiaxial loading where the plastic deformations occur is currently an area of active research. For reasonable estimates are possible for relatively simple situations, but there is some uncertainty exists as to the best procedure for complex non-proportional loadings, where the ratios of the principal stresses change, and where the principal axes may also rotate. Given this situation, the discussion that follows first considers some simple, but limited methods. Then an introductory discussion is given of possible approaches for more complex loadings.

5.3.1 EFFECTIVE STRAIN APPROACH

The fatigue for multiaxial loading is postulated to depend on the value of this effective strain amplitude for uniaxial loading

$$\varepsilon_a = \frac{\sigma'_f}{E}\left(2N_f\right)^b + \varepsilon'_f\left(2N_f\right)^c \quad (5.1)$$

where the first and second terms correspond to elastic and plastic strain components.

This approach was used for loading case A

5.4 CRITICAL PLANE APPROACH

This critical plane approach is valid for proportional loading and non-proportional loading to a significant degree. In such an approach, stresses and strains during cyclic loading are determined for different orientations (planes) within the material, and therefore the stresses and strains acting on the foremost severely loaded plane are wanted to predict fatigue failure.

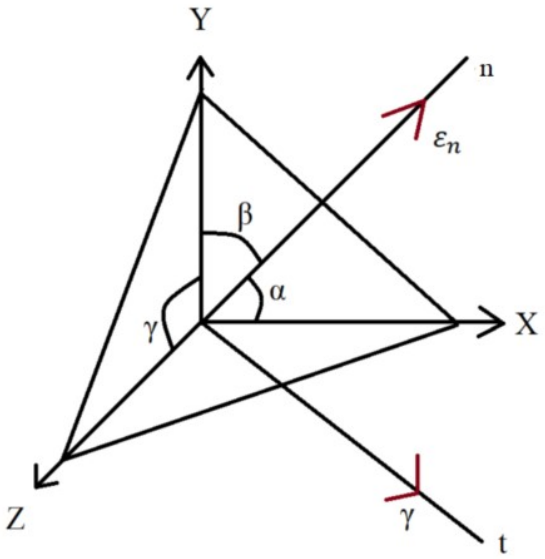

Figure 20 Critical Plane

Damage parameter on the critical plane can be a shear strain, normal strain, and normal stress for individuals loading cases see figure:21,22and23. It is seen that γ_{max} and ε_n are the figure:(21) in-phase, and the amplitude of ε_n^* is smaller. And figure:22 and figure:23 is the relation for the phase angle conditions φ = 45° and φ = 90°, respectively under the same equivalent strain applied. It may be seen that the change for the amplitude of γ_{max} is not large, but the amplitude of ε_n obviously increases with the phase angle.

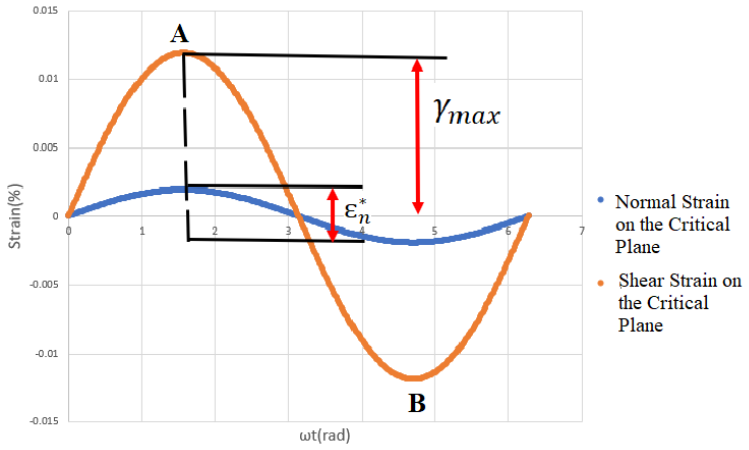

Figure 21 in-Phase Loading

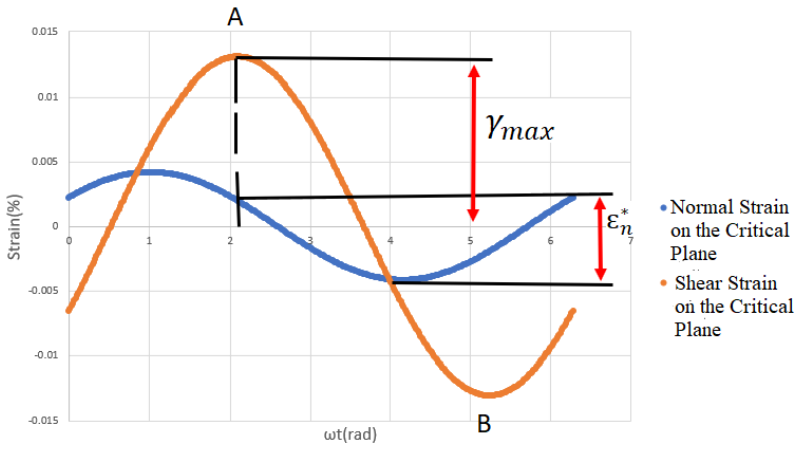

Figure 22 45°out-of-Phase Loading

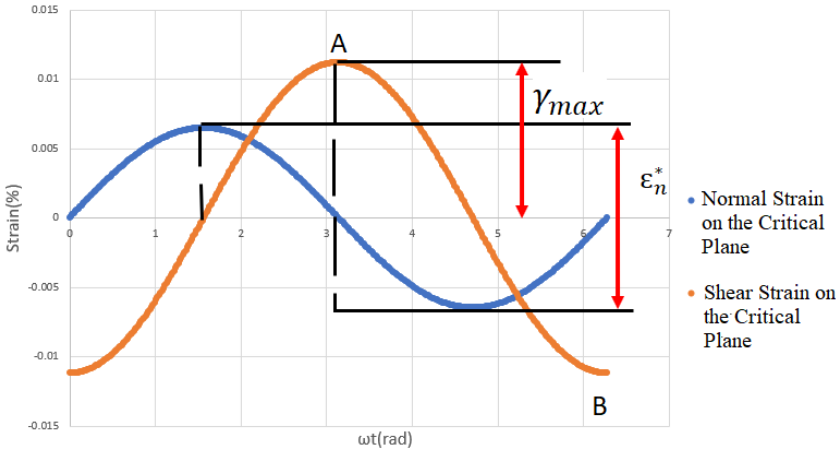

Figure 23 90°out-of-Phase Loading

From the figure: 21, 22 and 23 is the varying characteristic of the shear strain and the normal strain on the critical plane (valid for specimens C3 -proportional, H3- phase angle 45°= $\frac{\pi}{4}$ degrees, G3 -90°= $\frac{\pi}{2}$ degrees).

From the figure:24,25 and 26 is an evident variation of damage parameter on the critical plane (valid for specimens C3 -proportional, H3- phase angle 45°= $\frac{\pi}{4}$ degrees, G3 -90°= $\frac{\pi}{2}$ degrees).

(A)

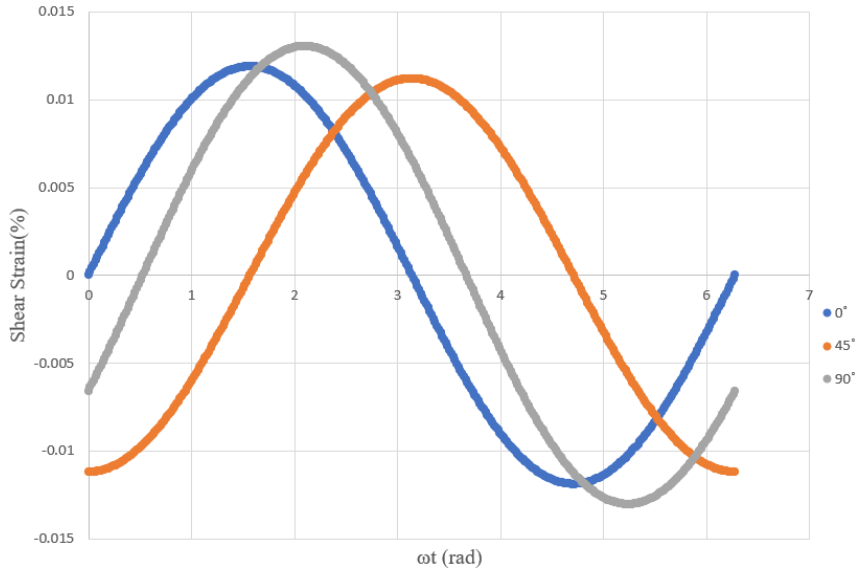

Figure 24 Variation of Shear Strain on Critical Plane

(B)

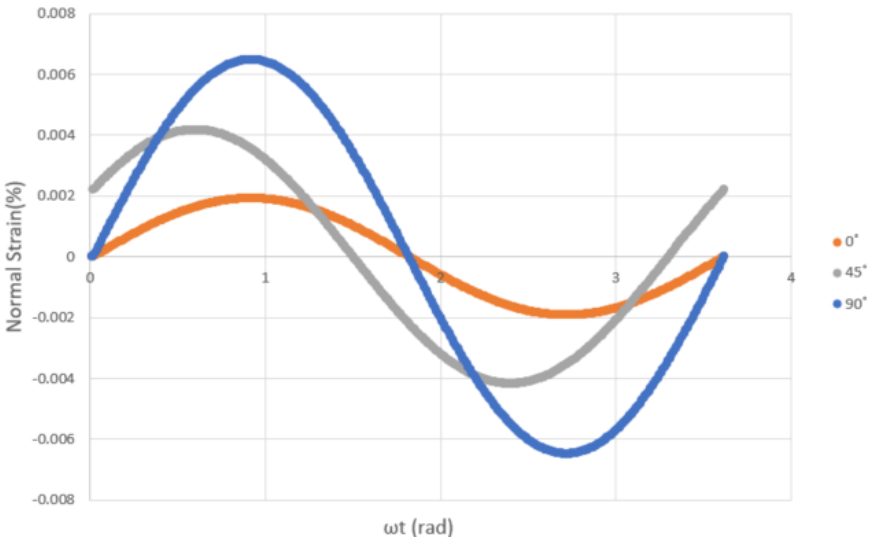

Figure 25 Variation of Normal Strain on Critical Plane

(C)

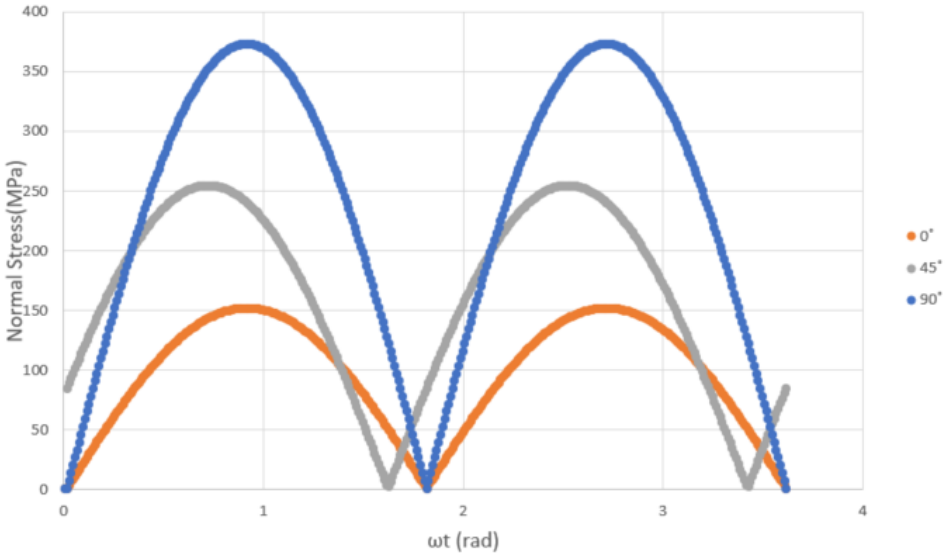

Figure 26 Variation of Normal Stress on Critical Plane

5.5 CRITICAL PLANE STRAIN APPROACHES

The critical plane approach usually utilizes the maximum shear plane as the critical damage plane. γ_{max} and ε_n on the critical plane are used to make the two basic parameters forming the fatigue damage parameter.

5.5.1 BROWN- MILLER CRITERION

In this model, the critical plane in which the maximum value occurs is taken from shear deformation. The Brown-Miller criterion is described by the relation.[9]

$$\frac{\Delta\gamma_{max}}{2} = \frac{\tau'_f}{G}\left(2N_f\right)^{b_\gamma} + \gamma'_f\left(2N_f\right)^{c_\gamma} \tag{5.2}$$

Where $\Delta\gamma_{max}$ is the maximum shear strain range. G is the shear modulus of elasticity, τ'_f shear fatigue strength coefficient, γ'_f shear fatigue ductility coefficient, respectively and c_γ torsion fatigue ductility exponent and b_γ are the torsion fatigue strength exponent. N_f shows the number of cycles to failure.

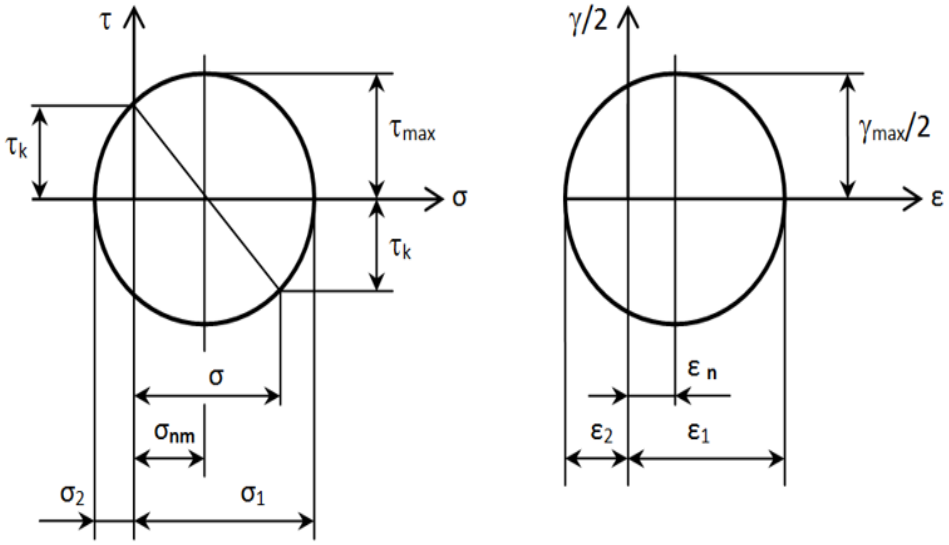

Figure 27 a) Mohr's Circle for Stress and b) Mohr's Circle for Strain

This approach was used for specimen B, C, G, and H

5.5.2 KANDIL-BROWN-MILLER CRITERION

It is like the Brown-Miller criterion, which includes the components of normal as well as shear deformation. The criterion is expressed by the relation.[12]

$$\frac{\Delta\bar{\gamma}}{2} = \left(\frac{\Delta\gamma_{max}^{\alpha}}{2} + S\Delta\varepsilon_n^{\alpha}\right)^{\frac{1}{\alpha}} = f(N_f) \tag{5.3}$$

Where $\triangle\gamma_{max}$ is the maximum shear strain range. S is the material constant, which expresses influence ε_n to crack growth and is determined from tensile torsion test and the $\triangle\varepsilon_n$ is range of normal strain at the critical plane. To determine the lifetime, the expression of the Kandil-Brown-Miller criterion can be written in the form.

$$\frac{\Delta\bar{\gamma}}{2} = \left(\frac{\Delta\gamma_{max}^{\alpha}}{2} + S\Delta\varepsilon_n^{\alpha}\right)^{\frac{1}{\alpha}} = \frac{\tau_f'}{G}(2N_f)^{b_\gamma} + \gamma_f'(2N_f)^{c_\gamma} \tag{5.4}$$

Where G is the shear modulus of elasticity, τ_f' shear fatigue strength coefficient, γ_f' shear fatigue ductility coefficient, respectively and c_γ shear fatigue ductility exponent, b_γ shear fatigue strength exponent. N_f shows the number of cycles to failure.

5.5.3 WANG-BROWN CRITERION

This criterion was created by modifying the Kandil-Brown-Miller criterion to include the effect of mean stress.[13]

$$\frac{\Delta\bar{\gamma}}{2} = \frac{\Delta\gamma_{max}}{2} + S\Delta\varepsilon_n = f(N_f) \tag{5.5}$$

Fatigue life of specimen can then be determined from the following relationship:

$$\frac{\Delta\gamma_{max}}{2} + S\Delta\varepsilon_n = A\frac{\sigma_f' - \sigma_{nm}}{E}\left(2N_f\right)^b + B\varepsilon_f'\left(2N_f\right)^c \tag{5.6}$$

where σ_{nm} is the normal mean stress on the critical plane and constants A and B are the expressed using a relationship (5.7,5.8)

$$A = 1.3+0.7S \tag{5.7}$$

$$B = 1.5+0.5S \tag{5.8}$$

5.5.4 SHANG-WANG CRITERION

It is based on the Manson-Coffin relation, where the values of strain amplitude and effect of normal stress are considered according to the hypothesis for use in multiaxial loading. This criterion is rather applicable in the case of proportional or in-phase loading. When applied to non-proportional loading, this criterion gives us distorted values.[10]

$$\left[\frac{1}{3}(\Delta\gamma_{max}/2)^2 + \Delta\varepsilon_n^2\right]^{\frac{1}{2}} = \frac{\sigma_f' - \sigma_{nm}}{E}\left(2N_f\right)^b + \varepsilon_f'\left(2N_f\right)^c \tag{5.9}$$

5.6 STRESS- STRAIN APPROACHES OF THE CRITICAL PLANE

The use of those criteria is both for the Low-cycle fatigue but also for the High-cycle fatigue in contrast to the strain criteria. The most member of the strain-stress criteria is that the strain as a control element and only after that the stress. Mean normal stress can play a large role within the lifetime of a component, and therefore its effect is included. The decisive factor is the direction of this stress on the critical plane.

5.6.1 FATEMI-SOCIE CRITERION

The Fatemi-Socie criterion is one of the most widely used and has great application for the shear damage model. The formulation of this criterion is as follows.[13][14]

$$\frac{\Delta\gamma}{2}\left(1 + k\frac{\sigma_{n,max}}{\sigma_y}\right) = f\left(N_f\right) \tag{5.10}$$

Where $\triangle\gamma$ is the maximum shear strain range, k is representing the material constant the determined from tensile and torsional test data, k=0.4,1.0 and 0.2 and $\sigma_{n,max}$ is the maximum normal stress. σ_y is the material yield limit.

To determine the life of the specimen equation can be written in the form (5.10)

$$\frac{\Delta\gamma}{2}\left(1 + k\frac{\sigma_{n,max}}{\sigma_y}\right) = \frac{\acute{\tau_f}}{G}\left(2N_f\right)^{b_\gamma} + \acute{\gamma_f}\left(2N_f\right)^{c_\gamma} \tag{5.11}$$

Where $\acute{\tau_f}$ is the shear fatigue strength coefficient and $\acute{\gamma_f}$ is the shear fatigue ductility coefficient, and b_γ and c_γ are express the shear fatigue strength and shear fatigue ductility exponents, respectively and G is the shear modulus.

5.7 ENERGY APPROACHES OF THE CRITICAL PLANE

The criteria contained within the energy approach are based on the assumption that the decisive influence on the lifetime of the component has the total energy accumulated until the moment of fracture. For one load cycle, this energy corresponds to the area of the hysteresis loop. As we move around the Low-cycle fatigue, these criteria will be suitable for us.

5.7.1 SMITH-WATSON-TOPPER CRITERION

In this tensile damage model, due to Smith-Watson-Topper for its the ability to account for the effects of cyclic hardening and softening. It predicts by the fatigue crack plane is the plane orientation with the maximum normal stress (the maximum principal stress). The S-W-T criterion for multiaxial fatigue loading is based on the $\triangle\varepsilon_1$ maximum principal of strain range and $\sigma_{n,max}$ is the maximum normal stress on the $\triangle\varepsilon_1$ plane. The Smith-Watson-Topper criterion is given in the form[15]

$$\sigma_{n,max}\frac{\Delta\varepsilon_1}{2} = \varepsilon_f'\sigma_f'\left(2N_f\right)^{c+b} + \frac{\sigma_f'^{\,2}}{E}\left(2N_f\right)^{2b} \tag{5.12}$$

Where σ_f' is the fatigue strength coefficient, ε_f' is the fatigue ductility coefficient, and b, c is express the fatigue strength exponent and fatigue ductility exponent.

5.7.2 LIU'S VIRTUAL STRAIN-ENERGY CRITERION

Liu developed a virtual criterion of the deformation energy, which may be a generalization of the axial energy on the idea of prediction of fatigue life. During this Criterion considers has two possible failure modes. The first mode for tensile failure, $\triangle W_1$ and the second mode for shear failure, $\triangle W_2$. The failure is predicted to occur on the material plane having the almost virtual strain-energy quantity. $\triangle W_1$ is calculated by firstly determining the plane on which the axial work is maximized and then adding the respective shear work on that same plane. And also, similarly $\triangle W_2$ is calculated by firstly determining the plane on which the shear work is maximized and then adding the respective axial work on that same plane. Criterion has the following form.[13]

$$\Delta W_I = (\Delta\sigma_n\Delta\varepsilon_n)_{max} + (\Delta\tau\Delta\gamma) \tag{5.13}$$

$$\Delta W_I = 4\sigma_f'\varepsilon_f'\left(2N_f\right)^{b+c} + \frac{4\tau_f'^{\,2}}{G}\left(2N_f\right)^{2b} \tag{5.14}$$

Similarly, ΔW_{II} is calculated by firstly determining the plane on which the shear work is maximized then adding the axial work thereon same plane. Eq: (5.15) and fatigue life are often achieved considering Eq: (5.16)

$$\Delta W_{II} = (\Delta\sigma_n \Delta\varepsilon_n) + (\Delta\tau\Delta\gamma)_{max} \quad (5.15)$$

$$\Delta W_{II} = 4\tau_f'\gamma_f'(2N_f)^{b+c} + \frac{4\tau_f'^2}{G}(2N_f)^{2b} \quad (5.16)$$

Where $\triangle\sigma_n$ and $\triangle\varepsilon_n$ are the normal stress range and normal strain range, respectively. $\triangle\tau$ and $\triangle\gamma$ are the shear stress range and shear strain range, ε_f' is the fatigue ductility coefficient and σ_f' is the fatigue strength coefficient respectively, τ_f' is the shear fatigue strength coefficient and γ_f' is the shear fatigue ductility coefficient, and b, c is express the fatigue strength exponent and fatigue ductility exponent.

5.7.3 CHEN'S CRITERION

In the case of Chen's criterion, is postulated that both normal and shear components of stress and strain on the critical plane contribute to the damage within the materials. For the material showing normal fracture, the almost maximum principal normal strain plane is taken into the critical plane, the fatigue criterion is given as follows[16][17]

Normal fracture:

$$W = \triangle\varepsilon_{1max}\triangle\sigma_1 + \triangle\gamma_1\triangle\tau_1 = 4\frac{\sigma_f'^2}{E}(2N_f)^{2b} + 4\sigma_f'\varepsilon_f'(2N_f)^{b+c} \quad (5.17)$$

For the shear mode failure, is the maximum shear strain plane is taken as the critical plane. The model is given by the following criterion.

Shear fracture:

$$W = \triangle\gamma_{max}\triangle\tau + \triangle\varepsilon_n\triangle\sigma_n = 4\frac{\tau_f'^2}{G}(2N_f)^{2b_t} + 4\tau_f'\gamma_f'(2N_f)^{b_t+c_t} \quad (5.18)$$

In this equation (5.17,5.18) the density of deformation energy in the critical plane W is expressed, where $\triangle\varepsilon_{1max}$ is the maximum principal strain range, and $\triangle\sigma_1$, $\triangle\gamma_1$ and $\triangle\tau_1$ are respectively, the normal stress range, shear strain range, and shear stress range that occur on the maximum principal strain range plane. where $\triangle\gamma_{max}$ is the maximum shear strain range, and $\triangle\tau$, $\triangle\varepsilon_n$, and $\triangle\sigma_n$ are the respectively, shear stress range, normal strain range, and normal stress range on the maximum shear strain plane, respectively.

5.7.4 VARANI-FARAHANI CRITERION

The Varani-Farahani is recommended as energy-based in the multiaxial fatigue parameter. The parameter is given by the sum of the normal strain energy and the shear strain energy measured on the critical plane where the stress and strain Mohr circles are the largest during the loading and the unloading parts of the cycle. The normal and shear energies in this parameter have been used to weight by the axial and shear fatigue properties, respectively. The proposed parameter takes into account the effect is the sum of the normal energy range and the shear energy range calculated for the critical plan.[18]

The parameter is given by

$$\frac{1}{\sigma'_f\varepsilon'_f}(\triangle\sigma_n \triangle\varepsilon_n) + \frac{(1+\sigma_n^{m}/\sigma'_f)}{\tau'_f\gamma'_f}\left(\triangle\tau_{max}\triangle\left(\frac{\gamma_{max}}{2}\right)\right) = f(N_f) \tag{5.19}$$

Where the normal mean stress σ_n^m acting on the critical plane and σ'_f and ε'_f are the axial fatigue strength coefficient and axial fatigue ductility coefficient, respectively and τ'_f and γ'_f are the shear fatigue strength coefficient and shear fatigue coefficient respectively, $\triangle\tau_{max}$ is the range of maximum shear stress and $\triangle(\gamma_{max}/2)$ shear strain, respectively and $\triangle\sigma_n$ and $\triangle\varepsilon_n$ are the normal stress range and normal strain range.

5.7.5 GLINKA CRITERION

The Glinka has proposed a fatigue parameter by using the sum of strain energy density in the critical plane to be.[19]

$$W = \frac{\Delta\gamma_{12}}{2}\frac{\Delta\sigma_{12}}{2} + \frac{\Delta\varepsilon_{22}}{2}\frac{\Delta\sigma_{22}}{2} \tag{5.20}$$

Where the parameter W is representing the fraction of the strain energy composed of the stresses and strains on the critical plane. By considering the mean stress effect, a modified formulation associated with the critical plane was proposed by Glinka in the following form.

$$W^* = \frac{\Delta\gamma_{12}}{2}\frac{\Delta\sigma_{12}}{2}\left[\frac{1}{1-\sigma_{12}^{max}/\tau'_f} + \frac{1}{1-\sigma_{22}^{max}/\sigma'_f}\right] = A(N_f)^b + C(N_f)^d \tag{5.21}$$

Where σ_{12}^{max} and σ_{22}^{max} are the maximum absolute values of shear and normal stresses in the critical plane, respectively, A, b, C, d are constants of the materials, and σ'_f and τ'_f are the axial

and torsional cyclic fatigue strength coefficients, respectively, $\Delta\gamma_{12}$ and $\Delta\sigma_{12}$ are the shear strain and shear stress ranges on the critical plane.

5.7.6 PAN WEN-FANG CRITERION

According to Pan Wen-Fang et al. (PHC) is changed the Glinka parameter and that suggested a parameter weighted by based on axial and shear fatigue properties.[15]

$$W' = \frac{\Delta\gamma_{12}}{2}\frac{\Delta\sigma_{12}}{2} + k_1\frac{\Delta\varepsilon_{22}}{2}\frac{\Delta\sigma_{22}}{2} \tag{5.22}$$

Where k_1 is the weight constant and is given by

$$k_1 = \frac{\acute{\gamma}_f}{\acute{\varepsilon}_f}\frac{\acute{\sigma}_f}{\acute{\tau}_f} \tag{5.23}$$

The parameter is given by Equation:(5.19) and (5.20) yielded good correlation with the fatigue lives in their respective for a number of the materials. In view of Equation:(5.18) and considering the mean stress effect, this energy-based on fatigue criteria can be written as:

$$\left(1 + \frac{\sigma_n^m}{\acute{\sigma}_f}\right)\frac{\Delta\gamma_{12}}{2}\frac{\Delta\sigma_{12}}{2} + k_1\frac{\Delta\varepsilon_{22}}{2}\frac{\Delta\sigma_{22}}{2} = \frac{\tau_f'^2}{G}\left(2N_f\right)^{2b_t} + 4\sigma_f'\varepsilon_f'\left(2N_f\right)^{b_t+c_t} \tag{5.24}$$

For the PHC model, are

$$k_2\Delta\sigma_n\Delta\varepsilon_n + \left(1 + \frac{\sigma_n^m}{\acute{\sigma}_f}\right)\frac{\Delta\gamma_{12}}{2}\frac{\Delta\sigma_{12}}{2} + k_1\frac{\Delta\varepsilon_{22}}{2}\frac{\Delta\sigma_{22}}{2} = \frac{\tau_f'^2}{G}\left(2N_f\right)^{2b_t} + 4\sigma_f'\varepsilon_f'\left(2N_f\right)^{b_t+c_t} \tag{5.25}$$

Where k_2 is the weight constant and is given by

$$k_2 = \frac{\acute{\tau}_f}{\acute{\sigma}_f}\frac{\acute{\gamma}_f}{\acute{\varepsilon}_f} \tag{5.26}$$

Where $k_1 = \acute{\gamma}_f/\acute{\varepsilon}_f$ and $k_2 = \acute{\tau}_f/\acute{\sigma}_f$ are two weight constants for strain and stress amplitudes, respectively, $\Delta\varepsilon_{22}$ and $\Delta\sigma_{22}$ are the normal strain and normal stress range in the critical plane.

6.RESULTS OF INDIVIDUALS APPROACHES AND COMPARISON WITH EXPERIMENT

6.1 LOADING CASE A-PUSH PULL

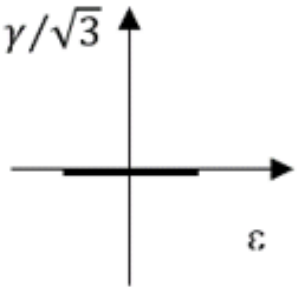

Figure 28 Push-Pull

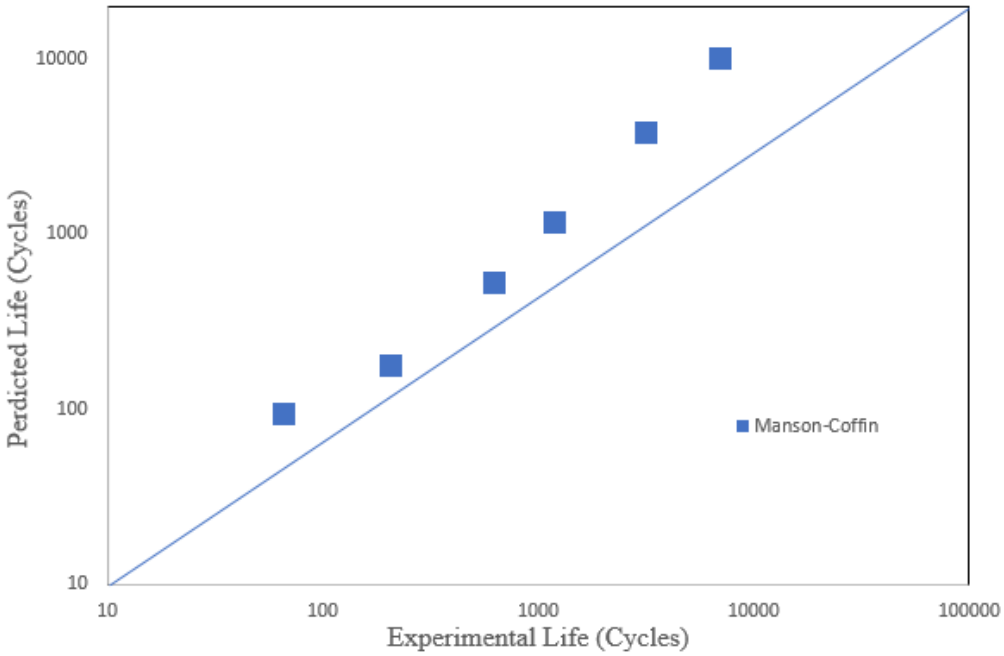

Figure 29 Predicted versus Experimental for Push-Pull

Eight specimens were used for case A-Push-pull loading. For this situation, Manson-Coffin equation was used. Comparison with the experiment-see figure:29. This method gives good results only for smaller fatigue life, for larger fatigue life some scatter exists. It should be noted that there is a variance for all materials parameters.

6.2 LOADING CASE B-PURE TORSION

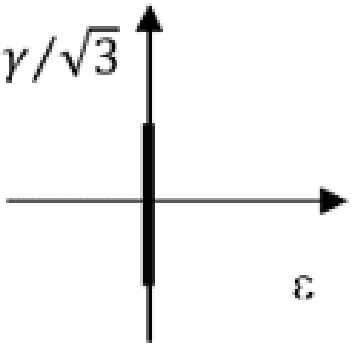

Figure 30 Pure Torsion

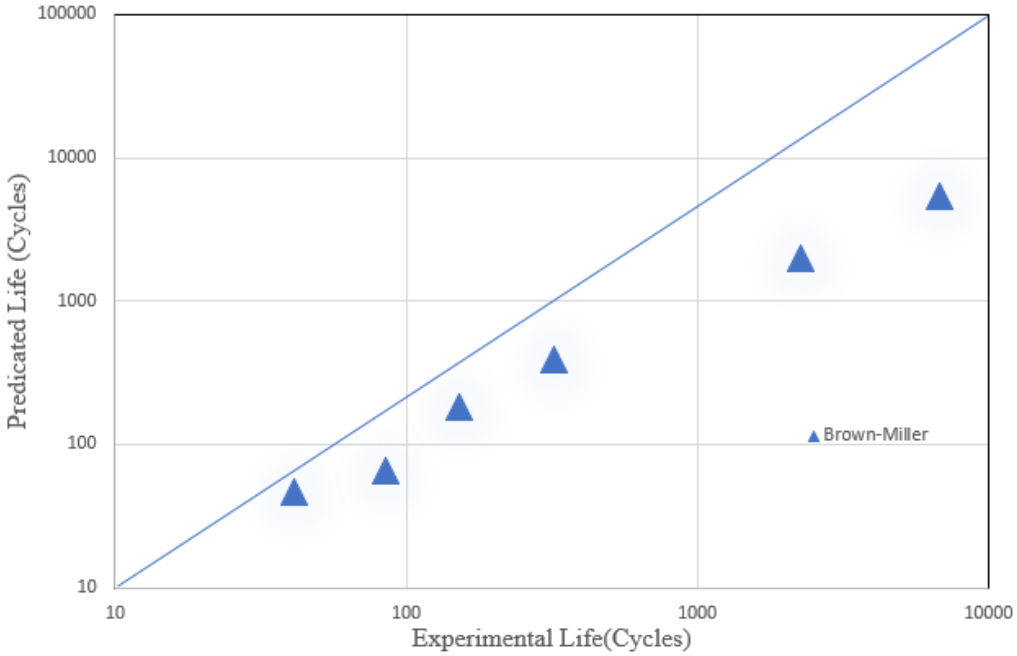

Figure 31 Predicted versus Experimental for Torsion

Eight specimens were used for case B-Pure torsion loading. For this situation, Brown-Miller equation was used. Comparison with the experiment- see figure: 31. A good correlation exists again for smaller fatigue life.

6.3 LOADING CASE C – PROPORTIONAL LOADING

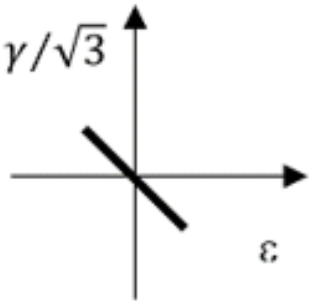

Figure 32 in-phase

For this proportional loading effort to verify the proposed model is following methods were used. BM, WB, KBM, FS and SWT models were conducted and the experiments were carried out under various loading. The loading history and loading path under proportional loading for the fatigue tests.

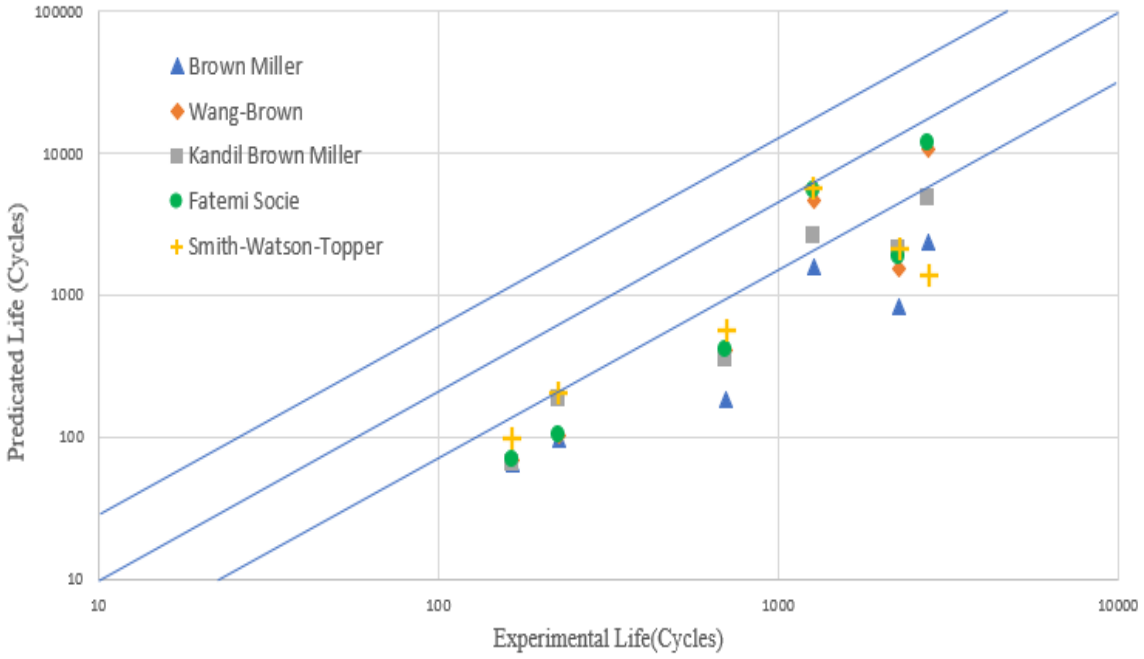

Figure 33 Predicted versus Experimental for Proportional Loading

Eight specimens were used for case C-Proportional Loading. Several methods were used for this situation – see figure:33. After starting some different loading cases and comparison with the experiment the number of cycles to failure for different models of the loading damage. The good results are given method by Kandil-Brown-Miller, Wang- Brown, and Fatemi-Socie.

6.4 LOADING CASE G- OUT-OF-PHASE ANGLE 90°, NON-PROPORTIONAL LOADING

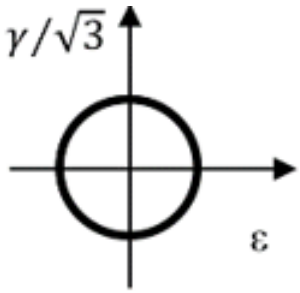

Figure 34 out-of-phase angle 90°

For this non-proportional loading effort to verify the proposed model is following methods were used. BM, WB, KBM, FS and SWT models were conducted and the experiments were carried out under various loading. The loading history and loading path under out-of-phase angle 90° non-proportional loading for the fatigue tests.

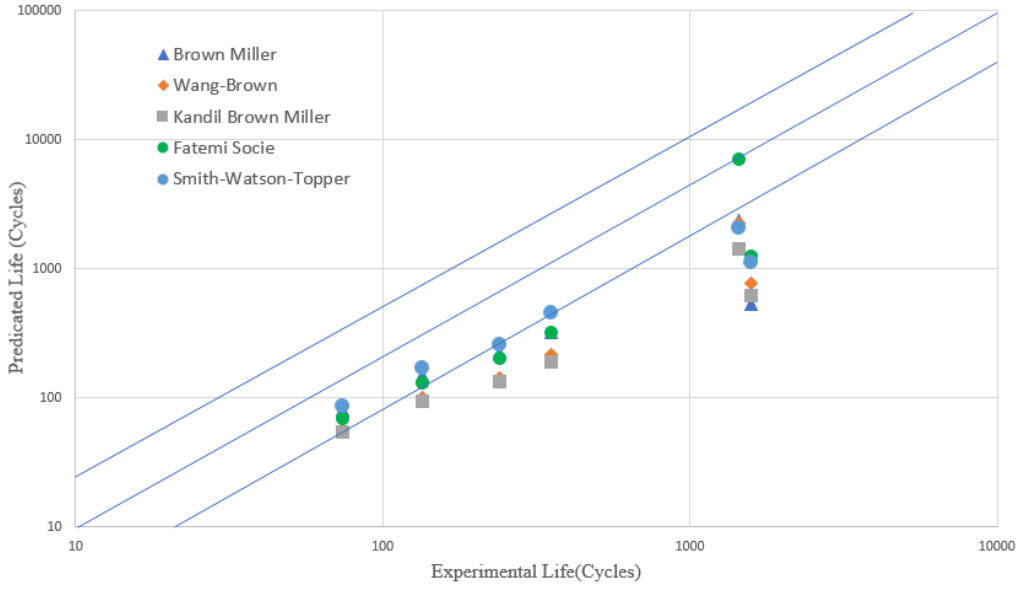

Figure 35 Predicted versus Experimental for 90° Non-Proportional Loading

Eight specimens were used for case G- out-of-Phase angle 90° non-proportional loading. Several methods were used for this situation–see figure:35. After starting some different loading cases and comparison with the experiment the number of cycles to failure for different models of the loading damage. The good results are given methods by Fatemi-Socie and Smith-Watson-Topper.

6.5 LOADING CASE H- OUT-OF-PHASE ANGLE 45°, NON-PROPORTIONAL LOADING

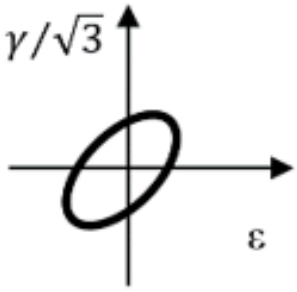

Figure 36 out-of-phase angle 45°

For this non-proportional loading effort to verify the proposed model is following methods were used. BM, WB, KBM, FS and SWT models were conducted and the experiments were carried out under various loading. The loading history and loading path under out-of-phase angle 45° non-proportional loading for the fatigue tests.

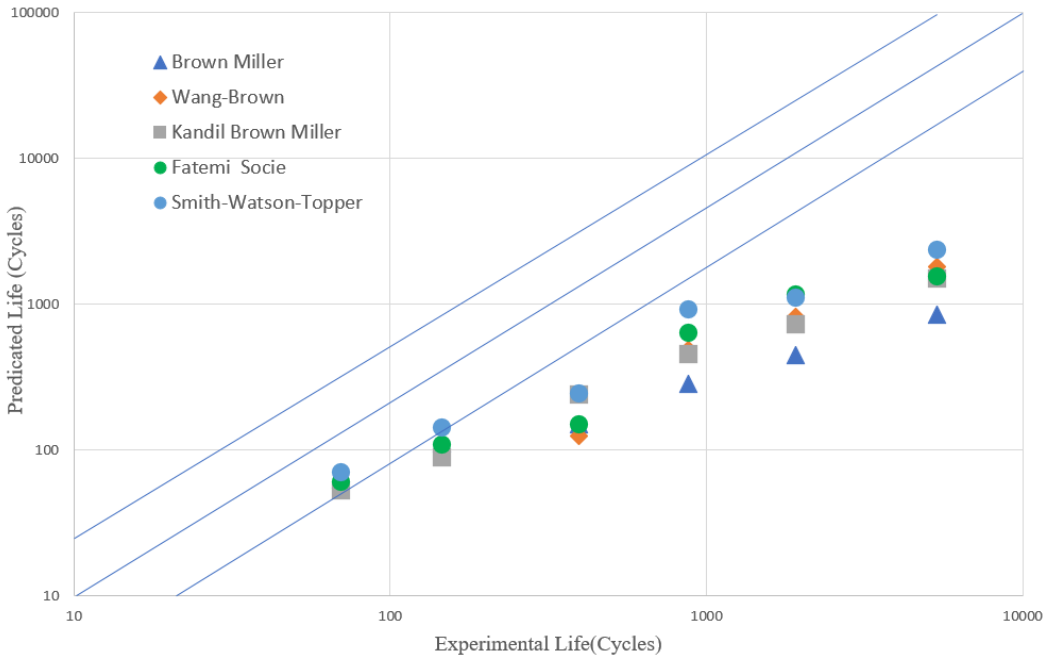

Figure 37 Predicted versus Experimental for 45° Non-Proportional Loading

Eight specimens were used for case H- out-of-phase angle 45° non-proportional loading. Several methods were used for this situation–see figure:37. After starting some different loading cases and comparison with the experiment the number of cycles to failure for different models of the loading damage. The good results are given methods by Fatemi-Socie and Smith-Watson-Topper.

7. CONCLUSIONS

The diploma thesis addressed the issue of predicting the life of components at multiaxial fatigue. The aim of this work was the determination of fatigue life of some specimens for different loading cases and comparison with the experiment. A low-cycle fatigue damage model applied to multiaxial loading of thin-walled tubes was proposed. The proposed fatigue damage model was based on the critical plane concept, and the equivalent strain was made with the maximum shear range $\triangle\gamma_{max}$, the normal strain range $\triangle\varepsilon_n$, and the maximum normal stress $\sigma_{n,max}$. The normal strain excursion between adjacent turning points of the maximum shear strain on the critical plane is an important parameter affecting multiaxial fatigue damage. And analyses indicate that ε_n and γ_{max} are in-phase under proportional loading and they are out-of-phase under non-proportional loading. Every multiaxial criterion applied to the fatigue lifetime calculation of aluminum alloy AA2124-T851 and also values of the number of cycles to failure from experiments increases with decreasing strain amplitude continuously in the cycles of number region.

The further stress-strain approach was used for the determination of fatigue life. For this situations, Fatemi-Socie parameter reasonably good results estimated from proportional and non-proportional loading. The Wang-Brown parameter is found to be somewhat conservative for proportional loading. Further energy approach was used for determination of fatigue life. For this situation, the Smith-Watson-Topper parameter, known to be more suitable for normal fracture materials, has relatively good performance for pure torsion and torsion-dominant strain paths. The prediction of service life is also influenced by fatigue parameters, which were expressed for selected types of load paths by using calculations in Mathcad Software and Microsoft Excel Software. The result values are shown in Annexures.

The goal of this thesis is the determination of fatigue life in multiaxial fatigue loading. The life prediction model was established by the proposed multiaxial fatigue damage parameter. The results have been shown that the critical plane criterion gives a good correlation of multiaxial fatigue damage parameter can be used for various proportional and non-proportional loading conditions for different specimen's fatigue data. It is very convenient for engineering applications.

8.REFERENCE

[1] Material Fatigue Definition. (2021). Retrieved 12 April 2021, from https://www.comsol.com/multiphysics/material-fatigue?parent=structural-mechanics-0182-242

[2] DOWLING,N.E. Mechanical behavior of materials. Engineering Methods for Deformation, Fracture and fatigue. Third edition. Pearson Prentice Hall,2007. ISBN 0-13-186312-6.

[3] Download Phenomenological Approaches to Moral Philosophy: A Handbook. (2021). Retrieved 24 April 2021, from http://defensorvlopez.gov.ar/html2pdf/locale/lib.php?q=download-Phenomenological-Approaches-to-Moral-Philosophy%3A-A-Handbook.html

[4] KUČERA,J. Úvod do mechaniky lomu. Únava materiálu. VŠB-TU Ostrava,1994. 80s. Skriptum. ISBN 80-7078-244-7. (Vlastnosti zkouseni materialu, VSB Ostrava 2013)

[5] When materials are getting tired… - ppt video online download. (2021). Retrieved 24 April 2021, from https://slideplayer.com/slide/1385676/

[6] Nondestructive Evaluation Physics: Materials. (2021). Retrieved 24 April 2021, from https://www.nde-ed.org/Physics/Materials/Mechanical/Fatigue.xhtml

[7] Fatigue and creep rapture. (2021). Retrieved 24 April 2021, from https://www.slideshare.net/umairbukhari3/fatigue-and-creep-rapture

[8] Fatigue (material) - Wikipedia. (2021). Retrieved 24 April 2021, from https://en.wikipedia.org/wiki/Fatigue_(material)

[9] LI, J, Z ZHANG, Q SUN, C LI a Y QIAO. A new multiaxial fatigue damage model for various metallic materials under the combination of tension and torsion loadings: Lecture Notes from the 2nd ERCOFTAC Summer schoolhel in Stockholm, 10-16 june, 1998. International Journal of Fatigue [online]. 2009, 31(4): 776-781 [cit. 2015-05-17]. DOI: 10.1016/j.ijfatigue.2008.03.008. ISSN 01421123. Dostupné z: http://linkinghub.elsevier.com/retrieve/pii/S0142112308000674

[10] DE-GUANG, S., & DE-JUN, W. (1998, July 01). A new multiaxial fatigue damage model based on the critical plane approach. Retrieved from https://www.sciencedirect.com/science/article/pii/S0142112397001230

[11] CHEN, H., SHANG, D., & BAO, M. (2010, December 14). Selection of multiaxial fatigue damage model based on the dominated loading modes. Retrieved from https://www.sciencedirect.com/science/article/pii/S0142112310003075

[12] WANG, Y., & YAO, W. (2005, September 02). A multiaxial fatigue criterion for various metallic materials under proportional and nonproportional loading. Retrieved from https://www.sciencedirect.com/science/article/pii/S014211230500174X

[13] (2021). Retrieved 25 April 2021, from https://www.researchgate.net/publication/262550020_Fatigue_behaviour_of_a_structural_steel_under_non-proportional_multiaxial_loading

[14] FATEMI, A., & SHAMSAEI, N. (2011, January 06). Multiaxial fatigue: An overview and some approximation models for life estimation. Retrieved from https://www.sciencedirect.com/science/article/pii/S0142112311000053

[15] HAN, C., CHEN, X., & KIM, K. (2002). Evaluation of multiaxial fatigue criteria under irregular loading. International Journal of Fatigue, 24(9), 913–922. https://doi.org/10.1016/s0142-1123(02)00013-0

[16] WANG, Y. (2004). Evaluation and comparison of several multiaxial fatigue criteria. International Journal of Fatigue, 26(1), 17–25. https://doi.org/10.1016/s0142-1123(03)00110-5

[17] CHEN, X., XU, S., & HUANG, D. (2003, November 05). A critical plane-strain energy density criterion for multiaxial low-cycle fatigue life under non-proportional loading. Retrieved from https://onlinelibrary.wiley.com/doi/full/10.1046/j.1460-2695.1999.t01-1-00199.x

[18] VARVANI-FARAHANI, A. (2000). A new energy-critical plane parameter for fatigue life assessment of various metallic materials subjected to in-phase and out-of-phase multiaxial fatigue loading conditions. *International Journal of Fatigue*, *22*(4), 295–305. https://doi.org/10.1016/s0142-1123(00)00002-5

[19] PAN, W.-F., HUNG, C.-Y., & CHEN, L.-L. (1999). Fatigue life estimation under multiaxial loadings. *International Journal of Fatigue*, *21*(1), 3–10. https://doi.org/10.1016/s0142-1123(98)00050-4

LIST OF ANNEXURES

Appendix 1 Mathcad calculation values for loading case A-Push-Pull using the method by Manson-Coffin equation was used.

Appendix 2 Mathcad calculation values for loading case B-Pure Torsion using the method by Brown-Miller equation was used.

Appendix 3 Mathcad calculation values for loading case C-Proportional loading using the method by BM, WB, KBM, FS and SWT equation was used. I have attached a Mathcad calculation for each method and, I have an several calculations for different specimens, Here I will show the calculation result of one specimen of each method from the Mathcad. And also list out the resultant value of every calculation methods of each specimens.

Appendix 4 Mathcad calculation values for loading case G- out-of-Phase angle 90° Non-Proportional Loading using the method by BM, WB, KBM, FS and SWT equation was used. I have attached a Mathcad calculation for each method and, I have an several calculations for different specimens, Here I will show the calculation result of one specimen of each method from the Mathcad. And also list out the resultant value of every calculation methods of each specimens.

Appendix 5 Mathcad calculation values for loading case H- out-of-Phase angle 45° Non-Proportional Loading using the method by BM, WB, KBM, FS and SWT equation was used. I have attached a Mathcad calculation for each method and, I have an several calculations for different specimens, Here I will show the calculation result of one specimen of each method from the Mathcad. And also list out the resultant value of every calculation methods of each specimens.

Appendix 1 Mathcad calculation values for loading case A-Push-Pull

(A1 – A6) – MANSON – C0FFIN

$x := 100$

$$\text{root}\left[\frac{611}{65540}\cdot(x)^{-0.063} + 0.529\cdot(x)^{-0.706} - 0.02, x\right] = 184.595 \qquad N := \frac{184.595}{2} = 92.297$$

$x := 100$

$$\text{root}\left[\frac{611}{65540}\cdot(x)^{-0.063} + 0.529\cdot(x)^{-0.706} - 0.015, x\right] = 344.851 \qquad N := \frac{344.851}{2} = 172.425$$

$x := 100$

$$\text{root}\left[\frac{611}{65540}\cdot(x)^{-0.063} + 0.529\cdot(x)^{-0.706} - 0.01, x\right] = 1.02 \times 10^{3} \qquad N := \frac{1.02 \times 10^{3}}{2} = 510$$

$x := 100$

$$\text{root}\left[\frac{611}{65540}\cdot(x)^{-0.063} + 0.529\cdot(x)^{-0.706} - 0.008, x\right] = 2.258 \times 10^{3} \qquad N := \frac{2.258 \times 10^{3}}{2} = 1.129 \times 10^{3}$$

$x := 100$

$$\text{root}\left[\frac{611}{65540}\cdot(x)^{-0.063} + 0.529\cdot(x)^{-0.706} - 0.0065, x\right] = 6.144 \times 10^{3} \qquad N := \frac{6.144 \times 10^{3}}{2} = 3.072 \times 10^{3}$$

$x := 100$

$$\text{root}\left[\frac{611}{65540}\cdot(x)^{-0.063} + 0.529\cdot(x)^{-0.706} - 0.0055, x\right] = 1.946 \times 10^{4} \qquad N := \frac{1.946 \times 10^{4}}{2} = 9.73 \times 10^{3}$$

Overall Result from Predicted versus Experimental for Push-Pull

Path A using by Manson-Coffin

Specimen number	Mathcad solution for N_f	Experiment N_f
A1	92.297	67
A2	172.425	209
A3	510	642
A4	$1.129x10^3$	1206
A5	$3072x10^3$	3194
A6	$9.73x10^3$	7062

Appendix 2 Mathcad calculation values for loading case B-Pure Torsion

B1-B6 - BROWN MILLER EQUATION

$$\text{root}\left[\frac{400}{26700}\cdot(x)^{-0.0978}+0.875\cdot(x)^{-0.874}-0.0264,x\right]=92.239 \qquad N:=\frac{92.239}{2}=46.12$$

$$\text{root}\left[\frac{400}{26700}\cdot(x)^{-0.0978}+0.875\cdot(x)^{-0.874}-0.0218,x\right]=129.291 \qquad N:=\frac{129.291}{2}=64.645$$

$$\text{root}\left[\frac{400}{26700}\cdot(x)^{-0.0978}+0.875\cdot(x)^{-0.874}-0.0135,x\right]=361.859 \qquad N:=\frac{361.859}{2}=180.929$$

$$\text{root}\left[\frac{400}{26700}\cdot(x)^{-0.0978}+0.875\cdot(x)^{-0.874}-0.0104,x\right]=781.801 \qquad N:=\frac{781.801}{2}=390.901$$

$$\text{root}\left[\frac{400}{26700}\cdot(x)^{-0.0978}+0.875\cdot(x)^{-0.874}-0.00730,x\right]=3.93\times10^{3} \qquad N:=\frac{3.93\times10^{3}}{2}=1.965\times10^{3}$$

$$\text{root}\left[\frac{400}{26700}\cdot(x)^{-0.0978}+0.875\cdot(x)^{-0.874}-0.00630,x\right]=1.082\times10^{4} \qquad N:=\frac{1.082\times10^{4}}{2}=5.41\times10^{3}$$

Overall Result from Predicted versus Experimental for Pure Torsion

Path B using by Brown-Miller

Specimen number	Mathcad solution for N_f	Experiment N_f
B1	46.12	41
B2	64.645	85
B3	180.929	152
B4	390.901	322
B5	$1.965x10^3$	2257
B6	$5.41x10^3$	6800

Appendix 3 Mathcad calculation values for loading case C-Proportional Loading

[1] Brown-Miller method using specimen for C1

$$x := 100$$

$$\text{root}\left[\frac{400}{26700}\cdot(x)^{-0.063} + 0.875\cdot(x)^{-0.706} - 0.039, x\right] = 131.148 \qquad N := \frac{131.148}{2} = 65.574$$

[2] Wang-Brown method using specimen for C1

PATH – C1

$$\lambda 1 := 1.732 \qquad x := 100$$

$$\alpha 1 := -0.322$$

$$\mu := 0.3$$

$$\varphi := 0$$

$$\gamma 1 := 0.039$$

$$\varepsilon 1 := 6.223\cdot 10^{-3}$$

$$TB1C1 := \frac{-\lambda 1\cdot\cos(2\alpha 1)\cdot\sin(\varphi)}{\lambda 1\cdot\cos(2\alpha 1\cdot\cos(\varphi)) - (1+\mu)\cdot\sin(2\alpha 1)} = 0$$

$$TB2C1 := \frac{\lambda 1\cdot\sin(2\alpha 1)\cdot\sin(\varphi)}{(1+\mu)\cdot\cos(2\alpha 1) + (1+\mu) + \lambda 1\cdot\sin(2\alpha 1\cdot\cos(\varphi))} = 0$$

$$\varepsilon c1 := \sqrt{\varepsilon 1^2 + \frac{1}{3}\cdot\left(\frac{\gamma 1}{2}\right)^2} = 0.013$$

$$\text{root}\left[\frac{611}{65540}\cdot(x)^{-0.0978} + 0.529\cdot(x)^{-0.874} - \varepsilon c1, x\right] = 138.527$$

$$N1 := \frac{138.527}{2} = 69.263$$

[3] Kandil-Brown-Miller method using specimen for C1

path c1

$s := 0.286$

$A := 1.3 + 0.7s = 1.5$

$B := 1.5 + 0.5s = 1.643$

$c1\gamma max := 0.039$

$c1\varepsilon n := 6.223 \cdot 10^{-3}$

$\sigma f := 611$

$E := 65540$

$b := -0.0978$

$c := -0.874$

$\varepsilon f := 0.529$

$x := 100$

$$\text{root}\left[A \cdot \frac{\sigma f}{E} \cdot (x)^{b} + B \cdot \varepsilon f \cdot (x)^{c} - \left(\frac{c1\gamma max}{2} + s \cdot c1\varepsilon n\right), x\right] = 127.305$$

$$N1 := \frac{127.305}{2} = 63.653$$

[4] Fatemi-Socie method using specimen for C1

path c1

$\sigma y := 435$

$\tau f := 400$

$G := 26700$

$b := -0.0978$

$c := -0.874$

$\gamma f := 0.875$

$k := 0.2$

$\gamma c1 := 0.039$

$c1\sigma nmax := 183.1$

$x := 100$

$$A1 := \frac{\gamma c1}{2}\left(1 + k \cdot \frac{c1\sigma nmax}{\sigma y}\right) = 0.021$$

$$\text{root}\left[\frac{\tau f}{G}(x)^{b} + \gamma f \cdot (x)^{c} - A1, x\right] = 136.872$$

$$N1 := \frac{136.872}{2} = 68.436$$

[5] Smith-Watson-Topper method using specimen for C1

path c1

$$\frac{2 \cdot 179}{323} = 1.108$$

$$\text{atan}(1.108) = 0.837$$

$$\sigma max := \frac{323}{2}(1 + \cos(0.837)) + 179 \cdot \sin(0.837) = 402.588$$

$$\frac{1 - 0.3}{2} \cdot 0.00889 + \frac{1.3}{2} \cdot 0.00889 \cdot \cos(0.837) + \frac{0.0154}{2} \cdot \sin(0.837) = 0.013$$

$$402.588 \cdot 0.013 = 5.234$$

$$x := 100$$

$$\text{root}\left[0.529 \cdot 611\,(x)^{-0.874-0.063} + \frac{611^2}{65540} \cdot (x)^{-2 \cdot 0.063} - 5.234, x\right] = 195.599$$

$$N1 := \frac{195.599}{2} = 97.799$$

Overall Result from Predicted versus Experimental for Proportional Loading

Path C using by Brown-Miller

Specimen number	Mathcad solution for N_f	Experiment N_f
C1	65.574	165
C2	96.838	226
C3	180.989	704
C4	841.5	2270
C5	1.566×10^3	1268
C6	2.384×10^3	2765

Wang-brown

Specimen number	Mathcad solution for N_f	Experiment N_f
C1	69.293	165
C2	103.028	226
C3	410.979	704
C4	1.513×10^3	2270
C5	4.713×10^3	1268
C6	1.054×10^4	2765

Kandil-Brown-Miller

Specimen number	Mathcad solution for N_f	Experiment N_f
C1	63.653	165
C2	184.9	226
C3	348.826	704
C4	2.096×10^3	2270
C5	2.559×10^3	1268
C6	4.809×10^3	2765

Fatemi-Socie

Specimen number	Mathcad solution for N_f	Experiment N_f
C1	68.436	165
C2	102.77	226
C3	413.244	704
C4	1.863×10^3	2270
C5	5.415×10^3	1268
C6	1.167×10^4	2765

Smith-Watson-Topper

Specimen number	Mathcad solution for N_f	Experiment N_f
C1	97.799	165
C2	207.155	226
C3	560.5	704
C4	2.142×10^3	2270
C5	5.64×10^3	1268
C6	1.385×10^3	2765

Appendix 4 Mathcad calculation values for loading case G- out-of-Phase angle90° Non-Proportional Loading

[1] Brown-Miller method using specimen for G1

$$\text{root}\left[\frac{400}{26700}\cdot(x)^{-0.063}+0.875\cdot(x)^{-0.706}-0.035,x\right]=161.79 \qquad N:=\frac{161.79}{2}=80.895$$

[2] Wang-Brown method using specimen for G1

PATH – G1

$G1\lambda1 := 1.733$

$G1\alpha1 := 0 \qquad x := 100$

$\mu := 0.3$

$\varphi := \frac{\pi}{2}$

$G1\gamma1 := 0.035$

$G1\varepsilon1 := 0.02$

$$TB1G1 := \frac{-G1\lambda1\cdot\cos(2G1\alpha1)\cdot\sin(\varphi)}{(G1\lambda1\cdot\cos(2G1\alpha1)\cdot\cos(\varphi))-(1+\mu)\cdot\sin(2G1\alpha1)}=-1.633\times10^{16}$$

$$TB2G1 := \frac{G1\lambda1\cdot\sin(2G1\alpha1)\cdot\sin(\varphi)}{(1+\mu)\cdot\cos(2\cdot G1\alpha1)+(1-\mu)+(G1\lambda1\cdot\sin(2\cdot G1\alpha1)\cdot\cos(\varphi))}=0$$

$G1\beta1 := \text{atan}(TB1G1) \qquad G1\beta2 := \text{atan}(TB2G1)$

$G1\beta1 = -1.571 \qquad G1\beta2 = 0$

$$G1\varepsilon n1 := \frac{1}{2}\cdot G1\varepsilon1\cdot(1+\cos(G1\beta1+G1\beta2))=0.01$$

$$G1\varepsilon c1 := \sqrt{G1\varepsilon n1^{2}+\frac{1}{3}\cdot\left(\frac{G1\gamma1}{2}\right)^{2}}=0.014$$

$$\text{root}\left[\frac{611}{65540}\cdot(x)^{-0.0978}+0.529\cdot(x)^{-0.874}-G1\varepsilon c1,x\right]=115.14$$

$$G1N1 := \frac{115.14}{2}=57.57$$

[3] Kandil-Brown-Miller method using specimen for G1

path g1

$s := 0.286$

$A := 1.3 + 0.7s = 1.5$

$B := 1.5 + 0.5s = 1.643$

$g1\gamma max := 0.035$

$g1\varepsilon n := 0.02$

$\sigma f := 611$

$E := 65540$

$b := -0.0978$

$c := -0.874$

$\varepsilon f := 0.529$

$x := 100$

$$\text{root}\left[A\cdot\frac{\sigma f}{E}\cdot(x)^{b} + B\cdot\varepsilon f\cdot(x)^{c} - \left(\frac{g1\gamma max}{2} + s\cdot g1\varepsilon n\right), x\right] = 109.163$$

$$N1 := \frac{109.163}{2} = 54.581$$

[4] Fatemi-Socie method using specimen for G1

path g1

$\sigma y := 435$

$\tau f := 400$

$G := 26700$

$b := -0.0978$

$c := -0.874$

$\gamma f := 0.875$

$k := 0.2$

$\gamma g1 := 0.035$

$g1\sigma nmax := 427$

$x := 100$

$$A1 := \frac{\gamma g1}{2}\left(1 + k\cdot\frac{g1\sigma nmax}{\sigma y}\right) = 0.021$$

$$\text{root}\left[\frac{\tau f}{G}(x)^{b} + \gamma f\cdot(x)^{c} - A1, x\right] = 139.411$$

$$N1 := \frac{139.411}{2} = 69.706$$

[5] Smith-Watson-Topper method using specimen for G1

g1

$$0.00998 \cdot 427 = 4.261$$

$$\text{root}\left[0.529 \cdot 611\,(x)^{-0.874-0.0978} + \frac{611^2}{65540} \cdot (x)^{-2 \cdot 0.0978} - 4.261, x\right] = 171.518$$

$$\frac{171.518}{2} = 85.759$$

Overall Result from Predicted versus Experimental for Non-Proportional Loading 90°

Path G using by Brown-Miller

Specimen number	Mathcad solution for N_f	Experiment N_f
G1	80.895	74
G2	150.778	135
G3	222.818	240
G4	325.006	352
G5	536	1580
G6	2.384×10^3	1445

Wang-Brown

Specimen number	Mathcad solution for N_f	Experiment N_f
G1	57.57	74
G2	101.986	135
G3	144.752	240
G4	216.99	352
G5	769.394	1580
G6	2.284×10^3	1445

Kandil-Brown-Miller

Specimen number	Mathcad solution for N_f	Experiment N_f
G1	54.581	74
G2	94.365	135
G3	132.715	240
G4	190.448	352
G5	625.266	1580
G6	1.417×10^3	1445

Fatemi-Socie

Specimen number	Mathcad solution for N_f	Experiment N_f
G1	69.706	74
G2	132.405	135
G3	204.403	240
G4	321.523	352
G5	1.255×10^3	1580
G6	7.05×10^3	1445

Smith-Watson-Topper

Specimen number	Mathcad solution for N_f	Experiment N_f
G1	85.759	74
G2	169.875	135
G3	260.163	240
G4	454.257	352
G5	1.133×10^3	1580
G6	2.091×10^3	1445

Appendix 5 Mathcad calculation values for loading case H- out-of-Phase angle 45° Non-Proportional Loading

[1] Brown-Miller method using specimen for H1

$$\text{root}\left[\frac{400}{26700}\cdot(x)^{-0.063}+0.875\cdot(x)^{-0.706}-0.04,x\right]=124.989 \qquad N:=\frac{124.989}{2}=62.495$$

[2] Wang-Brown method using specimen for H1

PATH – H1

$H1\lambda1 := 1.733$ $x := 100$

$H1\alpha1 := -0.295$

$\mu := 0.3$

$\varphi := \frac{\pi}{4}$

$H1\gamma1 := 0.04$

$H1\varepsilon1 := 0.013$

$$TB1H1 := \frac{-H1\lambda1\cdot\cos(2H1\alpha1)\cdot\sin(\varphi)}{(H1\lambda1\cdot\cos(2H1\alpha1)\cdot\cos(\varphi))-(1+\mu)\cdot\sin(2H1\alpha1)}=-0.585$$

$$TB2H1 := \frac{H1\lambda1\cdot\sin(2H1\alpha1)\cdot\sin(\varphi)}{(1+\mu)\cdot\cos(2\cdot H1\alpha1)+(1-\mu)+(H1\lambda1\cdot\sin(2\cdot H1\alpha1)\cdot\cos(\varphi))}=-0.621$$

$H1\beta1 := \text{atan}(TB1H1)$ $H1\beta2 := \text{atan}(TB2H1)$

$H1\beta1 = -0.529$ $H1\beta2 = -0.555$

$$H1\varepsilon n1 := \frac{1}{2}\cdot H1\varepsilon1\cdot(1+\cos(H1\beta1+H1\beta2))=9.537\times10^{-3}$$

$$H1\varepsilon c1 := \sqrt{H1\varepsilon n1^{2}+\frac{1}{3}\cdot\left(\frac{H1\gamma1}{2}\right)^{2}}=0.015$$

$$\text{root}\left[\frac{611}{65540}\cdot(x)^{-0.0978}+0.529\cdot(x)^{-0.874}-H1\varepsilon c1,x\right]=104.916$$

$$H1N1 := \frac{104.916}{2}=52.458$$

[3] Kandil-Brown-Miller method using specimen for H1

path h1

$s := 0.286$

$A := 1.3 + 0.7s = 1.5$

$B := 1.5 + 0.5s = 1.643$

$h1\gamma max := 0.04$

$h1\varepsilon n := 0.013$

$\sigma f := 611$

$E := 65540$

$b := -0.0978$

$c := -0.874$

$\varepsilon f := 0.529$

$x := 100$

$$root\left[A\cdot\frac{\sigma f}{E}\cdot(x)^{b} + B\cdot\varepsilon f\cdot(x)^{c} - \left(\frac{h1\gamma max}{2} + s\cdot h1\varepsilon n\right), x\right] = 105.249$$

$$N1 := \frac{105.249}{2} = 52.624$$

[4] Fatemi-Socie method using specimen for H1

path h1

$\sigma y := 435$

$\tau f := 400$

$G := 26700$

$b := -0.0978$

$c := -0.874$

$\gamma f := 0.875$

$k := 0.2$

$\gamma h1 := 0.04$

$h1\sigma nmax := 283.7$

$x := 100$

$$A1 := \frac{\gamma h1}{2}\left(1 + k\cdot\frac{h1\sigma nmax}{\sigma y}\right) = 0.023$$

$$root\left[\frac{\tau f}{G}(x)^{b} + \gamma f\cdot(x)^{c} - A1, x\right] = 120.967$$

$$N1 := \frac{120.967}{2} = 60.483$$

[5] Smith-Watson-Topper method using specimen for H1

path h1

$$0.00998\sqrt{\left(2\cdot 1.3\cdot\cos(0.4155)^2-2\cdot 0.3+1.733\cdot\sin(0.8258)\cdot\cos\left(\frac{\pi}{4}\right)\right)^2+\left(1.733\cdot\sin(0.8311)\cdot\sin\left(\frac{\pi}{4}\right)\right)^2}=0.026$$

$$475.015\cdot 0.026=12.35$$

$$\frac{12.35}{2}=6.175$$

$$\text{root}\left[0.529\cdot 611\,(x)^{-0.874-0.063}+\frac{611^2}{65540}\cdot(x)^{-2\cdot 0.063}-6.175,x\right]=141.396$$

$$\frac{141.396}{2}=70.698$$

Overall Result from Predicted versus Experimental for Non-Proportional Loading 45°

Path H using by Brown-Miller

Specimen number	Mathcad solution for Nf	Experiment Nf
H1	62.495	70
H2	110.659	146
H3	150.778	396
H4	283.552	874
H5	445.502	1912
H6	841.5	5360

Wang-Brown

Specimen number	Mathcad solution for Nf	Experiment Nf
H1	52.458	70
H2	91.1	146
H3	124.624	396
H4	486.686	874
H5	819.47	1912
H6	1.799×10^3	5360

Kandil-Brown-Miller

Specimen number	Mathcad solution for Nf	Experiment Nf
H1	52.624	70
H2	89.374	146
H3	240.608	396
H4	452.532	874
H5	731.909	1912
H6	1.499×10^3	5360

Fatemi-Socie

Specimen number	Mathcad solution for Nf	Experiment Nf
H1	60.483	70
H2	107.953	146
H3	302.061	396
H4	636.113	874
H5	1.174×10^3	1912
H6	1.555×10^3	5360

Smith-Watson-Topper

Specimen number	Mathcad solution for Nf	Experiment Nf
H1	70.698	70
H2	141.626	146
H3	242.716	396
H4	918.5	874
H5	1.099×10^3	1912
H6	2.364×10^3	5360